Journal of the Mechanics and Physics of Solids 107 (2017) 294–319

Contents lists available at ScienceDirect

Journal of the Mechanics and Physics of Solids

journal homepage: www.elsevier.com/locate/jmps

# Thermal fluctuations and effective bending stiffness of elastic thin sheets and graphene: A nonlinear analysis

Fatemeh Ahmadpoor[a], Peng Wang[b], Rui Huang[b], Pradeep Sharma[a,c,*]

[a] Department of Mechanical Engineering, University of Houston, Houston, TX 77204, USA
[b] Department of Aerospace Engineering and Engineering mechanics, University of Texas, Austin, TX 78712, USA
[c] Department of Physics, University of Houston, Houston, TX 77204, USA

ARTICLE INFO

*Article history:*
Received 30 May 2017
Revised 1 July 2017
Accepted 11 July 2017
Available online 12 July 2017

*Keywords:*
Graphene
Thermal fluctuations
Nonlinear elasticity
Variational perturbation method

ABSTRACT

The study of statistical mechanics of thermal fluctuations of graphene—the prototypical two-dimensional material—is rendered rather complicated due to the necessity of accounting for geometric deformation nonlinearity. Unlike fluid membranes such as lipid bilayers, coupling of stretching and flexural modes in solid membranes like graphene leads to a highly anharmonic elastic Hamiltonian. Existing treatments draw heavily on analogies in the high-energy physics literature and are hard to extend or modify in the typical contexts that permeate materials, mechanics and some of the condensed matter physics literature. In this study, using a variational perturbation method, we present a "mechanics-oriented" treatment of the thermal fluctuations of elastic sheets such as graphene and evaluate their effect on the effective bending stiffness at finite temperatures. In particular, we explore the size, pre-strain and temperature dependency of the out-of-plane fluctuations, and demonstrate how an elastic sheet becomes effectively stiffer at larger sizes. Our derivations provide a transparent approach that can be extended to include multi-field couplings and anisotropy for other 2D materials. To reconcile our analytical results with atomistic considerations, we also perform molecular dynamics simulations on graphene and contrast the obtained results and physical insights with those in the literature.



## 1. Introduction

Just over a decade ago, the first atomically thin crystalline material, graphene, was discovered (Novoselov et al., 2005). An entirely new field of research centered around the so-called 2D materials has emerged since then (Akinwande, et al., 2017; Bhimanapati et al., 2015; Butler et al., 2013). Beyond graphene, other examples of 2D materials that have now been made in the laboratories include molybdenum disulphide, phosphorene, boron nitride and many others. Their geometrical and mechanical characteristics along with other associated physical properties have opened up fascinating new application avenues ranging from electronics, energy harvesting, biological systems, structural composites among others (Ahmadpoor and Sharma, 2015; Akinwande, et al., 2017; Kim et al., 2009; Kostarelos and Novoselov, 2014). Ironically, rather than potential applications, after the initial discovery of graphene the issue that ignited most interest in the scientific community in the early years was related to whether 2D materials should even exist at all (Mermin, 1968). The famous Mermin–Wagner

* Corresponding author at: Department of Mechanical Engineering, University of Houston, Houston, TX 77204, USA.
*E-mail address:* psharma@uh.edu (P. Sharma).

http://dx.doi.org/10.1016/j.jmps.2017.07.011
0022-5096/

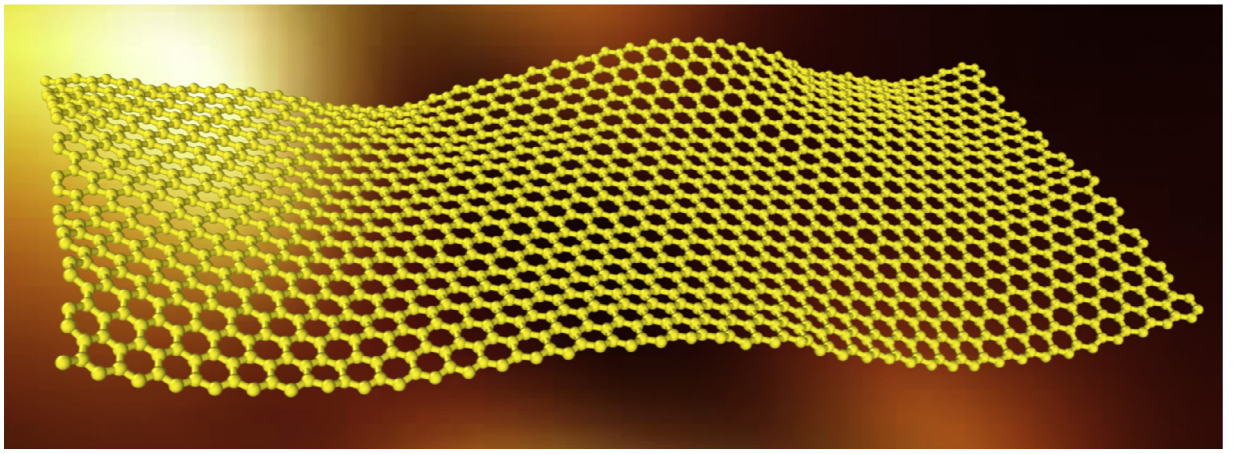

**Fig. 1.** Snapshot of molecular dynamics simulation of a graphene monolayer illustrating pronounced thermal fluctuations at room temperature.

theorem[1] (Mermin, 1968), taught in standard condensed matter text-books, prohibits the existence of stable 2D crystalline materials. A rich literature has since emerged that has focused on thermal fluctuations of graphene and other 2D materials (Fasolino et al., 2007; Meyer et al., 2007) and is now recognized that while graphene does indeed exhibit noticeable thermal fluctuations or undulations, nonlinear elasticity—specifically, the coupling between bending deformation and stretching—has a stabilizing effect on its fluctuations. Lipid bilayers (also termed fluid membranes) are arguably the counterparts of 2D crystalline materials in the soft matter world. Typical bending modulus ($\kappa_b$) of most lipid-bilayers is between 5 and $25k_BT$—small enough compared to the thermal energy scale that membranes undulate or fluctuate noticeably at physiological temperatures (Ahmadpoor and Sharma, 2017; Deserno, 2007; Nelson, 2004; Safran, 1994; Seifert, 1997). Bending rigidity of graphene at zero Kelvin, has been estimated to range from 1.2 to 1.6 eV (Koskinen and Kit, 2010; Kudin et al., 2001; Lu et al., 2009)—just a few times larger than the bending rigidity of biological membranes (at room temperature[2]). Thus, the energy cost for bending deformations of these materials is typically very low and at finite temperature, thermal undulations are well-evident,[3] as shown in Fig. 1.

Aside from fundamental scientific interest, thermal fluctuations of 2D materials are also of interest due to several other reasons. For example, in the biological context, many physiological processes are involved with thermal fluctuations of cell membranes, such as exo and endo-cytosis, membrane fusion, pore formation, cell adhesion, binding-unbinding transitions, self assembly, vesicle size selection among many others and this topic has now become one of the cornerstones of biophysical research (Ahmadpoor and Sharma, 2016; Auth et al., 2007; Farago and Santangelo, 2005; Fisher, 1993; Freund, 2013; Helfrich, 1986; Huang et al., 2017; Lipowsky and Leibler, 1986; Lipowsky and Seifert, 1991; Sharma, 2013). In the context of graphene, thermal fluctuations impact electronic properties, thermal conductivity and morphological transformations in finite sized ribbons (Kit et al., 2012; Lindsay et al., 2011; Morozov et al., 2008; Neto et al., 2009; Xu and Buehler, 2010). Interestingly, a more recent topic of growing interest involves the study of thermal fluctuations influencing the interactions of graphene with biological membranes (Gao, 2014; Li et al., 2013; Wang et al., 2013; Zhu et al., 2016).[4]

The elasticity of fluid membranes, at least in the linearized context, can be described by the Love–Kirchoff plate theory[5] and accordingly, their statistical mechanics study is relatively simple and the basic results (which we will summarize later in the paper) are well-established and widely available both in the archival literature as well as books (Boal and Boal, 2012; Phillips et al., 2012; Safran, 1994). 2D crystalline materials (—so called solid membranes) are harder to analyze. Unlike fluid

[1] The Mermin–Wagner theorem implies that 2D membranes in three-dimensional space undergo “wild” and long-range fluctuations which destroy its crystalline order.

[2] Even though both graphene and lipid bilayers bend easily, there are some key differences between the elastic behavior of fluid membranes (lipid bilayers) and solid membranes (such as graphene). Graphene’s larger “apparent” bending stiffness originates from the nonlinear coupling of in-plane stretching deformation and out-of-plane bending. This aspect will be discussed in depth in later sections.

[3] It is worthwhile to comment here that the study of thermal fluctuations in the context of soft matter has a longer history than graphene and other crystalline and/or solid 2D materials. The reader is referred to the following review papers Deserno (2007), Ahmadpoor and Sharma (2017) and Seifert (1997) and the books Nelson (2004), Nelson et al. (2004) and Boal and Boal (2012) that present a fascinating account of this topic.

[4] Such interactions have implications for several biomedical applications such as biosensors (Kuila et al., 2011), tissue scaffolds (Kalbacova et al., 2010; Nayak et al., 2011), carriers for drug delivery (Sun et al., 2008; Yang et al., 2011) and gene therapy (Feng et al., 2011). The graphene sheet undergoes thermal motion in the vicinity of the cellular membrane. Rather than adhering to cellular membrane, graphene sheet is observed to penetrate the bilayer, through one of its sharp corner (Li et al., 2013). This type of interaction (which does not change the total elastic energy) is primarily controlled by entropic effects arising from thermal undulations of both the membrane and the graphene sheet. Generally speaking, adhesion and cellular uptake of nano-materials, depending on their shapes and sizes, can be strongly affected by thermal fluctuations (Gao, 2014; Li et al., 2013; Wang et al., 2013).

[5] The elastic theory of fluid membrane may be interpreted to be a special case of Love–Kirchoff plate theory or perhaps it is more accurate to state that it is reminiscent of the Love–Kirchoff plate theory if the in-plane shear modulus is set to zero.

membranes, in addition to bending and stretching resistance, solid membranes may also exhibit non-trivial in-plane shear resistance. The in-plane deformations are nonlinearly coupled to the out-of-plane displacement field and the von-Karman nonlinear plate theory (Landau and Lifshitz, 1959) is usually employed to describe the elasticity of 2D solid membranes. Consideration of this nonlinearity is essential to obtain physically meaningful results for solid membranes. Unfortunately, this need to consider nonlinear elasticity renders an analytical study of the statistical mechanics of graphene and other analogous elastic sheets quite difficult. A substantive body of work exists in the physics literature where numerical Monte Carlo simulations, molecular dynamics and approximate analytical methods have been deployed to understand thermal fluctuations of graphene (Aronovitz and Lubensky, 1988; Doussal and Radzihovsky, 1992; Gao and Huang, 2014; Nelson and Peliti, 1987; Zakharchenko et al., 2010). Most of the treatments in the area of statistical mechanics of graphene and tethered membranes[6] find their origins in the developments in the high-energy physics literature (Amit and Martin-Mayor, 2005; Goldenfeld, 1992). Accordingly, those derivations are not readily understood by the mechanics and materials science community—despite the fact that the underlying basic starting point of the statistical mechanics analysis is nonlinear elasticity and of considerable interest to those communities.[7] Notable exceptions are recent works by Freund (2013) who presented a rather simple (but numerical) method based on Fourier series, and Liang and Purohit (2016a; 2016b) who used a finite element like numerical framework to discretize the membrane and then employed Gaussian integrals for the statistical mechanics. A nice advantage of the approach by Liang and Purohit (2016b) is the facile inclusion of boundary conditions for the fluctuations of finite membranes.

In this work, we:

(i) Present a variational approximation approach to develop the statistical mechanics of nonlinear elastic sheets such as graphene and obtain *closed-form* results.[8] Our approach is strongly connected to the concepts familiar to the mechanics and materials science community. It can be extended to situations not considered in the present work: coupling with non-mechanical fields, anisotropy among others. Finally, our approach yields the current state-of-the art derived using other highly specialized methods and presents a facile route for successively improving the accuracy of the approximation.

(ii) Present a one-dimensional toy model of the thermal fluctuations of a nonlinear solid membrane to explain in a transparent manner how the in-plane and out-of-plane deformations can be decoupled.

(iii) Derive closed-form expressions for the renormalized bending rigidity that, combined with the *bare* value of the bending modulus of graphene, captures the effects of nonlinearities. Our expression for renormalized bending rigidity shows that the in-plane elastic property (Young's modulus) of a solid sheet is indeed the dominant factor compared to the bare value of the bending modulus.

(iv) Incorporate the effect of pre-stretch in our derivations and provide insights into the effects of deformation nonlinearities in the presence of an in-plane tensile strain. Our closed-form expressions show that the stiffening effects of nonlinearities are suppressed when the membrane is under tensile strain—in agreement with previous Monte-Carlo and Molecular Dynamics simulations (Gao and Huang, 2014; Roldán et al., 2011).

(v) Perform molecular dynamics (MD) simulations on graphene and compare our theoretical predictions of out-of-plane fluctuations as a function of the size of the sheet. We further investigate the dependency of the renormalized bending stiffness on the size of sheet using MD and compare those with our theoretical predictions to explain how the solid membrane becomes effectively stiffer at larger sizes.

(vi) Explore the dependency of the fluctuations and renormalized bending rigidity on the temperature, using both the theoretical treatment and MD simulations. We show that, due to nonlinear effects, the fluctuations do not grow as predicted by the harmonic approximation. Our results suggest that the stiffening effect of nonlinearities becomes stronger at high-temperatures, and consequently, increases the renormalized bending rigidity.

The outline of this paper is as follows. In Section 2 an overview of the energy formulation of nonlinear elasticity is presented. Recognizing that the audience of our paper may have mixed background as far as statistical mechanics concerned, we briefly summarize some key pertinent concepts in Section 3. In particular, we also devise and discuss a toy model that is simply a one-dimensional analog of the actual problem of interest. In Section 4 we obtain a surprising result that despite the nonlinear nature of the problem, the 1D results can be evaluated exactly and are identical to the linearized 2D solution. We return to our original problem in Section 5 and present a variational approximation for deducing the thermal fluctuation spectra. The results of Section 5 are used to evaluate the effective bending stiffness in Section 6. Molecular dynamics simulations for fluctuations of graphene monolayers are performed for different sizes and temperatures and the details are provided in Section 7. We close our manuscript in Section 8 with a discussion of the results from our theoretical predictions, MD simulations and the literature.

[6] We remark that statistical mechanics of tethered or polymerized membranes can also be described analogous to graphene; at least in an continuum mechanics framework.

[7] No criticism is implied here. This is simply an observation that even for material scientists and mechanicians who have a reasonable understanding of statistical mechanics, Feyman's diagrams, renormalization group theory and related discipline specific etc. tend to be unfamiliar topics.

[8] Our emphasis is on analytical development and is complementary to efforts such as those of Liang and Purohit (2016a; 2016b). In principle, Monte Carlo or MD approaches can be used to obtain highly accurate results but are less transparent compared to analytical results and may be limited to relatively small sizes by computational costs.

## 2. Nonlinear elastic energy of isotropic thin elastic sheets and graphene

Consider a planar thin elastic sheet occupying a domain of size $\mathbb{S} = (0, L)^2$ in the $x - y$ plane and assume that at $T = 0\,\mathrm{K}$ (corresponding to the undeformed ground state), the membrane is situated on the $z = 0$ plane. Each point on the surface $\mathbb{S}$ is defined by its position vector $\mathbf{x}$. Let $\mathbf{u}$ be a vector field on $\mathbb{S}$, that describes the displacement field on the sheet and maps each point of the undeformed surface in 2D plane into a point on deformed surface in 3D coordinate. Then the position of each point on the deformed surface can be written as: $\mathbf{r} = \mathbf{x} + \mathbf{u}$. The transformation matrix for such deformation is defined as: $\mathbf{F} = \nabla_{2D}\mathbf{r}$, that transforms a 2D vector to a 3D vector. As a result of this deformation, the sheet may experience stretching (or compression) and bending. Typically, the first and second fundamental forms of the deformed surface are used to describe the stretching and bending deformations of an elastic sheet. The first fundamental form— the so-called metric tensor, $\mathbf{g}$— is associated with the areal change of the sheet. To build the metric tensor, we start with two tangent vectors on the deformed surface (Abbena et al., 2006):

$$\mathbf{a}_1 = \frac{\partial \mathbf{r}}{\partial x}, \qquad \mathbf{a}_2 = \frac{\partial \mathbf{r}}{\partial y} \tag{1}$$

Then, the first fundamental form is expressed as (Abbena et al., 2006): $g_{ij} = \mathbf{a}_i \cdot \mathbf{a}_j$, where $(i, j)$ runs between 1 and 2 and $g_{ij}$ is the $ij$ component of the metric tensor $\mathbf{g}$.[9] The Green–Lagrange strain field is a 2D tensor and can be written as (Gurtin et al., 2010; Lu and Huang, 2009):

$$\mathcal{E} = \frac{1}{2}(\mathbf{g} - \mathbf{I}). \tag{2}$$

where $\mathbf{I}$ is the 2D identity tensor. Assuming material isotropy,[10] the corresponding elastic energy cost for the strain field in (2) can be written as a function of its principal invariants, $I_1(\mathcal{E}) = \mathrm{tr}\ \mathcal{E}$ and $I_2(\mathcal{E}) = \det \mathcal{E}$ as[11]:

$$U_s = \int_{\mathbb{S}} \frac{E}{2(1-\nu^2)} I_1^2(\mathcal{E}) - \frac{E}{(\nu+1)} I_2(\mathcal{E}). \tag{3}$$

where $E$ and $\nu$ are the Young's modulus and Poisson ratio of the elastic sheet, respectively.

As a pure two-dimensional structure, a thin elastic sheet or graphene may exhibit (in principle) pure bending deformation without being stretched (or compressed). In the following we review the corresponding formulations for the bending deformation of an elastic sheet. The unit normal vector of the surface at any given point can be defined in terms of the two orthogonal surface tangent vectors (Abbena et al., 2006):

$$\mathbf{n} = \frac{\mathbf{a}_1 \times \mathbf{a}_2}{|\mathbf{a}_1 \times \mathbf{a}_2|} \tag{4}$$

from which the second fundamental form is obtained as: $b_{ij} = -\frac{\partial \mathbf{n}}{\partial x_j} \cdot \mathbf{a}_i$, where $x_i$ and $x_j$ denote the in-plane coordinate $x$ and $y$ and $b_{ij}$ are the $ij$-th component of the tensor $\mathbf{b}$. The curvature tensor is then obtained using the second fundamental form $\mathbf{b}$ and the inverse of the first fundamental form (Abbena et al., 2006):

$$\mathbf{L} = \mathbf{g}^{-1}\mathbf{b} \tag{5}$$

The principal curvatures[12] ($c_1$ and $c_2$) of the surface at a given point are then related to the invariants of the curvature tensor as (Abbena et al., 2006):

$$\begin{aligned} 2H &= c_1 + c_2 = \mathrm{tr}\mathbf{L} \\ K &= c_1 c_2 = \det\mathbf{L} \end{aligned} \tag{6}$$

where $H$ and $K$ are referred to as mean and Gaussian curvatures, respectively. The bending energy cost associated with this deformation may be described as a function of the invariants of the curvature tensor. Up to quadratic order, the bending energy is expressed as (Zhong-Can and Helfrich, 1989):

$$U_b = \int_{\mathbb{S}} \frac{1}{2}\kappa_b (c_1 + c_2)^2 + \kappa_G c_1 c_2. \tag{7}$$

where $\kappa_b$ and $\kappa_G$ are the bending moduli corresponding to mean and Gaussian curvatures. The energy function in Eq. (7) was first established in the context of the elastic theory of biological membranes by Helfrich (1973) and Canham (1970). Unlike the classical plate theory, where the bending moduli can be related to the Young's modulus and Poisson ratio, it is now well-recognized that for 2D materials such as graphene or even fluid membranes like lipid bilayers, the bending moduli

[9] It can be verified that the first fundamental form is related to the deformation gradient tensor as: $\mathbf{g} = \mathbf{F}^T\mathbf{F}$.

[10] The central ideas of this work can be readily extended to anisotropic 2D materials at the cost of tedious algebra.

[11] tr, denotes the trace operator and det, denotes the determinant of the tensor.

[12] Curvatures at a point can be evaluated in any direction but have a maximum and minimum values along two particular orthogonal directions. The corresponding maximum and minimum values of the curvature at a given point are referred to as the principal curvatures.

are best specified as independent properties (Lu et al., 2009) and may be evaluated by either experiments or microscopic methods such as atomistic simulations (Koskinen and Kit, 2010; Wei et al., 2012). Further, due to the Gauss–Bonnet theorem (Abbena et al., 2006), the integration of Gaussian curvature over a 2D *closed* area is fixed when the topology of the system does not change in the deformed configuration. This is certainly the case for the present study and in what follows, we disregard the second term in Eq. (7).[13]

We denote the components of the displacement field of the deformed sheet as: $\mathbf{u}(\mathbf{x}) = (u_x(\mathbf{x}), u_y(\mathbf{x}), w(\mathbf{x}))$. The in-plane strain field in Eq. (2) is a nonlinear function of the derivative of the displacement field. Since we consider extremely thin elastic sheets, such as graphene, the energy cost for in-plane deformation is significantly larger than the corresponding one for bending. Accordingly, the out-of-plane deformations are dominant. Hence, it is a reasonable approximation to neglect the nonlinear terms related to the *in-plane* displacement in the strain field in Eq. (2). With this approximation, the strain field may be rewritten as:

$$\mathcal{E}_{\gamma\delta} = \frac{1}{2}\left(\frac{\partial u_\delta}{\partial \gamma} + \frac{\partial u_\gamma}{\partial \delta} + \frac{\partial w}{\partial \gamma}\frac{\partial w}{\partial \delta}\right) \tag{8}$$

where the indices $\gamma$ and $\delta$ run between $x$ and $y$. Also, as long as the deviations from the flat state are small ($|\nabla w| \ll 1$), the linearized mean curvature ($H$) may be used and is described in terms of the out of plane displacement as follows:

$$2H = c_1 + c_2 = \frac{\partial^2 w}{\partial x^2} + \frac{\partial^2 w}{\partial y^2} = \nabla^2 w \tag{9}$$

The nonlinear strain tensor in Eq. (8), combined with the curvature definition in Eq. (9) results in a rather complicated form of the elastic energy. If the last term in Eq. (8) is neglected, then the in and out-of-plane deformations become uncoupled and the total elastic energy is strictly harmonic—i.e. a quadratic function of the curvatures and the derivatives of in-plane displacements. However, for most elastic sheets such as graphene, it is important to consider the nonlinear contribution of the out-of-plane displacement to the strain field in Eq. (8) which leads to the coupling between the in and out-of-plane deformations. The complexity and the anharmonicity appear in two parts; first, the contribution of the fourth order terms involving the out-of-plane deformation (as will be evident soon), and second, the coupling terms between the in-plane and out-of-plane displacements. Taking cognizance of this observation, we may split the total elastic energy into three parts: harmonic terms, $U_{\rm h}$, anharmonic terms dictating the coupling between in and out-of-plane displacement fields, $U_{\rm ac}$, and anharmonic terms $U_{\rm anh}$ involving purely the out-of-plane displacement. Hence we have:

$$U = U_b + U_s = \int_{\mathbb{S}} U_{\rm h} + U_{\rm ac} + U_{\rm anh} \tag{10}$$

in which

$$U_{\rm h} = \frac{1}{2}\kappa_b(\nabla^2\, w)^2 + \frac{E}{2(1-\nu^2)}\left(\left(\frac{\partial u_x}{\partial x}\right)^2 + \left(\frac{\partial u_y}{\partial y}\right)^2 + 2\nu\frac{\partial u_x}{\partial x}\frac{\partial u_y}{\partial y}\right) + \frac{E}{4(1+\nu)}\left(\frac{\partial u_x}{\partial y} + \frac{\partial u_y}{\partial x}\right)^2 \tag{11a}$$

$$U_{\rm ac} = \frac{E}{2(1-\nu^2)}\left(\frac{\partial u_x}{\partial x}\left(\frac{\partial w}{\partial x}\right)^2 + \frac{\partial u_y}{\partial y}\left(\frac{\partial w}{\partial y}\right)^2 + \nu\frac{\partial u_x}{\partial x}\left(\frac{\partial w}{\partial y}\right)^2 + \nu\frac{\partial u_y}{\partial y}\left(\frac{\partial w}{\partial x}\right)^2\right) + \frac{E}{2(1+\nu)}\frac{\partial w}{\partial x}\frac{\partial w}{\partial y}\left(\frac{\partial u_x}{\partial y} + \frac{\partial u_y}{\partial x}\right) \tag{11b}$$

$$U_{\rm anh} = \frac{E}{8(1-\nu^2)}\left(\left(\frac{\partial w}{\partial x}\right)^4 + \left(\frac{\partial w}{\partial y}\right)^4 + 2\left(\frac{\partial w}{\partial x}\frac{\partial w}{\partial y}\right)^2\right) = \frac{E}{8(1-\nu^2)}|\nabla w|^4 \tag{11c}$$

In what follows, we will study the statistical mechanics of the fully coupled nonlinear system including all the coupling and anharmonic terms in Eq. (11).

## 3. Key aspects of statistical mechanics of two-dimensional materials and the solution to harmonic approximation

Before analyzing the central problem described in the preceding sections, to provide a benchmark, we briefly (i) summarize the text-book solution for the harmonic case, and (ii) concoct a toy model to establish *some* of the key ideas. The

[13] We remark that this term cannot be disregarded if a *finite* sheet is considered since the Gaussian curvature does contribute to the conditions on the edge.

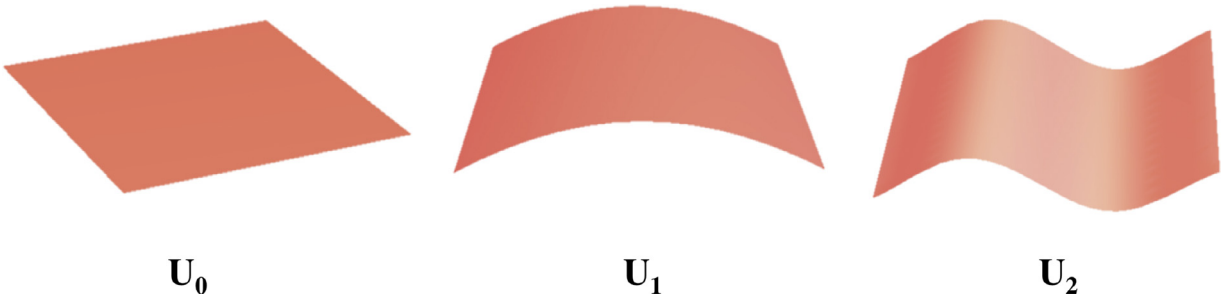


**Fig. 2.** Schematic of an elastic sheet that can have different modes of deformation at finite temperature. The probability of occurrence of each of these modes is proportional to the Boltzmann factor ($\propto \exp(-U_i/k_BT)$). The ground state that minimizes the energy is the most probable state, and deformation modes with higher energy cost are less probable.

toy model is essentially a 1D approximation to the actual problem we need to address. Somewhat surprisingly, we could not find this solution in the literature and is therefore an important benchmark calculation in its own right. Furthermore an exact solution can be obtained and, while this scenario is not realistic and misses important physics present in the full 2D situation, some key ideas become quite transparent. In particular, we also obtained an overlooked result that a fully anharmonic analysis of the 1D case is *identical* to the harmonic result of the 2D analysis.

The elastic energy cost to deform a planar elastic sheet is given in Eq. (11). At zero Kelvin, and in the absence of any external forces, the planar sheet would remain flat to minimize its total elastic energy. At finite temperature, however, due to thermal energy the sheet dynamically adopts non-flat shapes in a random manner that involve in and out-of-plane deformations (see Fig. 2). Each of these modes is associated with a probability distribution that (at finite temperature) is described by the Boltzmann factor (Kittel, 2004):

$$\rho_i \propto \exp(-U_i/k_BT)$$

where $k_BT$ is the thermal energy, $\rho_i$ is the probability of ocurrence of mode $i$ and $U_i$ is its associated energy. The probability distribution can be normalized to 1 through the normalizing factor $1/Z$, where $Z$ is the so-called partition function and is obtained by summing over all possible configurations (Kittel, 2004) which in this continuous system are uncountably infinite:

$$Z = \sum_i \exp(-U_i/k_BT) \tag{12}$$

The thermal probability distribution allows the computation of the ensemble average[14] of any physical quantity $\mathcal{X}$: (Kittel, 2004):

$$\langle \mathcal{X} \rangle = \sum_i \mathcal{X}_i \exp(-U_i/k_BT)$$

The planar sheet at finite temperature will remain in its equilibrium configuration (flat configuration) on *average*, however, will exhibit fluctuations around this equilibrium state. These fluctuations are related to the material properties as well as the size of the sheet. We consider first the harmonic analysis and this solution is widely available in several text-books c.f. (Nelson et al., 2004).

Consider a planar sheet of size $L^2$ in the $x-y$ plane. Neglecting in-plane deformation, we only focus on the out-of-plane undulations. The computation of the partition function in the context of field theories is greatly facilitated by going over to Fourier space and accordingly we proceed to transform the harmonic part of energy functional ($U_h$) by defining the following Fourier transformations of the out-of-plane displacement field $w(\mathbf{x})$:

$$w(\mathbf{x}) = \sum_{\mathbf{q}\in\mathbb{K}} \overline{w}(\mathbf{q}) \exp(\imath \mathbf{q}\cdot\mathbf{x}) \tag{13}$$

where $\mathbb{K} = \left\{\mathbf{q} : \mathbf{q} = \frac{2\pi}{L}(\nu_x, \nu_y),\ \nu_x, \nu_y \in \mathbb{Z},\ |\mathbf{q}| \in [q_{\min}, q_{\max}]\right\}$. Also, $\mathbf{q}$ is determined by the inverse of the wave-length, i.e. $\mathbf{q} = (\frac{2\pi}{l_x}, \frac{2\pi}{l_y})$, where $l_x$ and $l_y$ are the wave-lengths in $x$ and $y$ directions, respectively. In reality, the minimum wave-length of the fluctuations corresponds to the interatomic distance between the degrees of freedom. Let, $a$ be the smallest wave-length of fluctuations. Then $q_{\max} = 2\pi/a$ and $q_{\min} = 2\pi/L$. These expressions will be used later to calculate the fluctuations. The Fourier transform of the height function is then:

$$\overline{w}(q) = \frac{1}{L^2}\int_{\mathbb{S}} w(\mathbf{x})\mathbf{e}^{-\imath\mathbf{q}\cdot\mathbf{x}} d\mathbf{x} \tag{14}$$

[14] Due to the ergodic theorem (Kittel, 2004), the ensemble average is equivalent to time average at fixed temperature.

For the sake of completeness, we assume that the elastic sheet is also under an in-plane tensile pre-strain $\varepsilon_0$ along $x$ and $y$ directions. It can be then shown that when the sheet undergoes out-of-plane deformations the total elastic energy, up to quadratic order, is[15]:

$$\mathcal{U}_h = \int_{\mathbb{S}} \frac{1}{2}\kappa_b(\nabla^2\ w)^2 + \frac{E\varepsilon_0}{2(1-\nu)}|\nabla w|^2 \tag{15}$$

The elastic energy in (15), can be expanded in Fourier space as follows[16]:

$$\begin{aligned}\mathcal{U}_h &= \frac{1}{2}\sum_{\mathbf{q},\mathbf{q}'\in\mathbb{K}}\left(\kappa_b|\mathbf{q}|^2|\mathbf{q}'|^2 - \frac{E\varepsilon_0}{(1-\nu)}\mathbf{q}\cdot\mathbf{q}'\right)\overline{w}(\mathbf{q})\overline{w}(\mathbf{q}')\int e^{i(\mathbf{q}+\mathbf{q}')\cdot\mathbf{x}}d\mathbf{x}\\ &= \frac{1}{2}\sum_{\mathbf{q},\mathbf{q}'\in\mathbb{K}}\left(\kappa_b|\mathbf{q}|^2|\mathbf{q}'|^2 - \frac{E\varepsilon_0}{(1-\nu)}\mathbf{q}\cdot\mathbf{q}'\right)\overline{w}(\mathbf{q})\overline{w}(\mathbf{q}')L^2\delta(\mathbf{q},-\mathbf{q}')\\ &= \frac{L^2}{2}\sum_{\mathbf{q}\in\mathbb{K}}\left(\kappa_b|\mathbf{q}|^4 + \frac{E\varepsilon_0}{(1-\nu)}|\mathbf{q}|^2\right)|\overline{w}(\mathbf{q})|^2\end{aligned} \tag{16}$$

The partition function is calculated as:

$$\begin{aligned}Z &= \int_{-\infty}^{\infty}\exp\left(-\frac{L^2}{2k_BT}\sum_{\mathbf{q}\in\mathbb{K}}\left(\kappa_b|\mathbf{q}|^4 + \frac{E\varepsilon_0}{(1-\nu)}|\mathbf{q}|^2\right)|\overline{w}(\mathbf{q})|^2\right)\prod_{\mathbf{q}\in\mathbb{K}}d\overline{w}(\mathbf{q})\\ &= \prod_{\mathbf{q}\in\mathbb{K}}\sqrt{\frac{2\pi k_BT}{L^2|\mathbf{q}|^2\left(\kappa_b|\mathbf{q}|^2 + E\varepsilon_0/(1-\nu)\right)}}\end{aligned} \tag{17}$$

Then the average of the square of the amplitude in each mode is obtained as:

$$\begin{aligned}\langle|\overline{w}(\mathbf{q})|^2\rangle &= \frac{1}{Z}\int_{-\infty}^{\infty}|\overline{w}(\mathbf{q})|^2\exp\left(-\frac{L^2}{2k_BT}\sum_{\mathbf{q}'\in\mathbb{K}}\left(\kappa_b|\mathbf{q}'|^4 + \frac{E\varepsilon_0}{(1-\nu)}|\mathbf{q}'|^2\right)|\overline{w}(\mathbf{q}')|^2\right)\prod_{\mathbf{q}'\in\mathbb{K}}d\overline{w}(\mathbf{q}')\\ &= \frac{k_BT}{L^2\left(\kappa_b|\mathbf{q}|^4 + E\varepsilon_0|\mathbf{q}|^2/(1-\nu)\right)}\end{aligned}$$

More frequently, the phase averages are computed for harmonic systems by taking recourse to the so-called equipartition theorem (Aleksandr and Khinchin, 1949; Safran, 1994), which states that the thermal energy is equally shared among all the modes of deformations.[17] Accordingly, the average of the energy in each mode is:

$$\left\langle\frac{L^2}{2}\left(\kappa_b|\mathbf{q}|^4 + \frac{E\varepsilon_0}{(1-\nu)}|\mathbf{q}|^2\right)|\overline{w}(\mathbf{q})|^2\right\rangle := \frac{1}{2}k_BT \tag{18}$$

Consequently, the mean-square average of the fluctuations of each mode may be obtained as:

$$\langle|\overline{w}(\mathbf{q})|^2\rangle = \frac{k_BT}{L^2\left(\kappa_b|\mathbf{q}|^4 + E\varepsilon_0|\mathbf{q}|^2/(1-\nu)\right)} \tag{19}$$

In real space, the mean-square out-of-plane displacement is *both* the spatial and phase averages of the fluctuations at each point and can be evaluated as:

$$\begin{aligned}\langle w^2\rangle &= \frac{1}{L^2}\int_{\mathbb{S}}\langle w(\mathbf{x})^2\rangle d\mathbf{x}\\ &= \frac{1}{L^2}\sum_{\mathbf{q},\mathbf{q}'\in\mathbb{K}}\langle\overline{w}(\mathbf{q})\overline{w}(\mathbf{q}')\rangle\int_{\mathbb{S}}e^{i(\mathbf{q}+\mathbf{q}')\cdot\mathbf{x}}d\mathbf{x}\\ &= \sum_{\mathbf{q},\mathbf{q}'\in\mathbb{K}}\langle\overline{w}(\mathbf{q})\overline{w}(\mathbf{q}')\rangle\delta(\mathbf{q},-\mathbf{q}') = \sum_{\mathbf{q}\in\mathbb{K}}\langle|\overline{w}(\mathbf{q})|^2\rangle\end{aligned} \tag{20}$$

The summation in (20) can be evaluated using the following integration:

[15] Here, we neglect the ground state energy associated with the tensile pre-strain $\varepsilon_0$ which is inconsequential in what follows.

[16] Note that we have used the orthogonality property of the Fourier transformation that decouples the modes in a quadratic energy formulation. Also, note that $\overline{w}(-\mathbf{q}) = \overline{w}^*(\mathbf{q})$ are conjugates and hence we can set $\overline{w}(\mathbf{q})\overline{w}(-\mathbf{q}) = |\overline{w}(\mathbf{q})|^2$.

[17] This is however, valid *only* when the energy is a quadratic function of uncoupled degrees of freedom which is not the case for our problem of interest due to the presence of anharmonic terms.

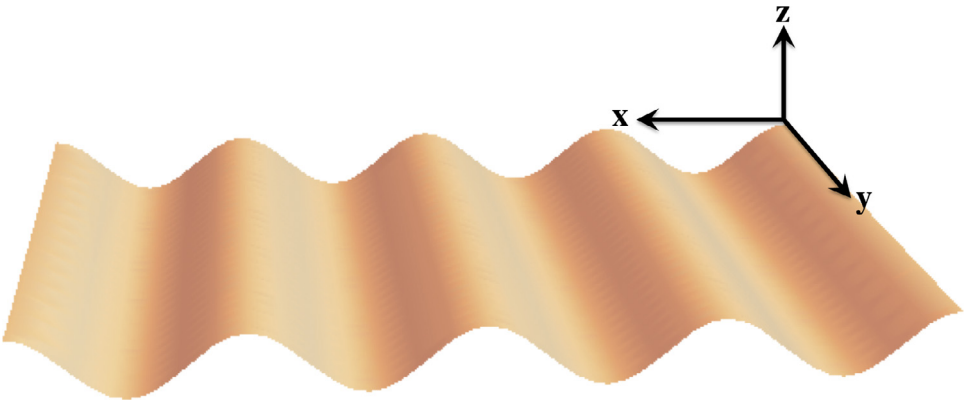


**Fig. 3.** Deformation of graphene sheet in one dimension. In this case, the displacement is only a function of $x$, and $u_y = 0$.

$$\begin{aligned}\langle w^2\rangle &= \sum_{\mathbf{q}\in\mathbb{K}}\langle|\overline{w}(\mathbf{q})|^2\rangle = \sum_{\mathbf{q}\in\mathbb{K}}\frac{k_BT}{L^2\left(\kappa_b|\mathbf{q}|^4+E\varepsilon_0|\mathbf{q}|^2/(1-\nu)\right)}\\ &= \left(\frac{L}{2\pi}\right)^2\int_{q_{\min}}^{q_{\max}}\frac{k_BT2\pi q}{L^2\left(\kappa_b q^4+E\varepsilon_0 q^2/(1-\nu)\right)}dq\\ &= \frac{k_BT}{4\pi E\varepsilon_0/(1-\nu)}\log\left(\frac{4\pi^2\kappa_b+L^2E\varepsilon_0/(1-\nu)}{4\pi^2\kappa_b+a^2E\varepsilon_0/(1-\nu)}\right)\end{aligned} \tag{21}$$

In the limit of $\varepsilon_0 \to 0$, the expression in (21) reduces to:

$$\begin{aligned}\langle w^2\rangle &\sim \frac{k_BT(L^2-a^2)}{16\pi^3\kappa_b}-\frac{k_BTE(L^4-a^4)}{128\pi^5\kappa_b^2(1-\nu)}\varepsilon_0+\mathcal{O}(\varepsilon_0^2)\\ &= \frac{k_BT(L^2-a^2)}{16\pi^3\kappa_b}\sim\frac{k_BTL^2}{16\pi^3\kappa_b},\qquad a\ll L\end{aligned} \tag{22}$$

The approximation of $a \ll L$ is fairly reasonable since the size of the sheet is usually much larger than the inter-atomic distances. Accordingly, the fluctuations of a tension-less elastic sheet, within the harmonic approximation, are proportional to its size, i.e. $\sqrt{\langle w^2\rangle} \propto L$. This simple correlation has been employed to extract the bending modulus of biological membranes from measured fluctuation spectra (Dimova, 2014; Engelhardt et al., 1985; Faucon et al., 1989; Pécréaux et al., 2004). We note that, as expected, introducing a non-zero tensile pre-strain results in the suppression of fluctuations. Further, when the sheet is under a non-zero tensile pre-strain, the relation of the fluctuations and the size of the sheet is different, and the fluctuations vary logarithmically with the size of sheet, i.e. $\langle w^2\rangle \propto \log L$, as noted in a previous work (Gao and Huang, 2014). In general however, for nonlinear elastic sheets such as graphene, these harmonic analysis estimations might be far from reality. In this paper, we aim to investigate a similar correlation between the fluctuations and the size of the sheet for nonlinear elastic sheets. We start with a simple one-dimensional toy model of the problem in the following section (Fig. 3).

## 4. Toy model: statistical mechanics of a nonlinear elastic sheet with 1D approximation

We now turn to a toy model which is essentially the fully nonlinear problem embodied in Eq. (11) albeit in a 1D approximation. To proceed with the 1D approximation, we artificially restrict the deformation such that the displacement field is solely a function of $x$ as: $(u_x, w) = (u_x(x), w(x))$ while $u_y = 0$. With this imposed restriction, the single component of the strain tensor becomes:

$$\mathcal{E}_x = \frac{\partial u_x}{\partial x}+\frac{1}{2}\left(\frac{\partial w}{\partial x}\right)^2+\varepsilon_0 \tag{23}$$

where, for the sake of completeness, we have considered a uniform tensile pre-strain $\varepsilon_0$ along the $x$ direction. Further, the bending and in-plane strain energy are reduced to:

$$U_b = \int\frac{1}{2}\kappa_b\left(\frac{\partial^2 w}{\partial x^2}\right)^2$$

$$U_s = \int\frac{E}{2(1-\nu^2)}\mathcal{E}_x^2$$

$$= \frac{1}{2}\bar{E}\int\left(\frac{\partial u_x}{\partial x}\right)^2 + \frac{\partial u_x}{\partial x}\left(\frac{\partial w}{\partial x}\right)^2 + \frac{1}{4}\left(\frac{\partial w}{\partial x}\right)^4 + 2\varepsilon_0\left(\frac{\partial u_x}{\partial x}\right) + \varepsilon_0\left(\frac{\partial w}{\partial x}\right)^2 + \varepsilon_0^2 \tag{24}$$

where we have set $\bar{E} = E/(1-\nu^2)$. As before with the harmonic case, we proceed to transform the energy functional by defining the following Fourier transformations of the displacement fields:

$$u_x(x) = \sum_{q\in\mathcal{K}_1} \bar{u}(q)\mathbf{e}^{iq\cdot x} \tag{25a}$$

$$w(x) = \sum_{q\in\mathcal{K}_1} \bar{w}(q)\mathbf{e}^{iq\cdot x} \tag{25b}$$

$$\left(\frac{\partial w}{\partial x}\right)^2 = \sum_{q\in\mathcal{K}_1} \bar{A}(q)\mathbf{e}^{iq\cdot x} \tag{25c}$$

where $\mathcal{K}_1 := \{q = 2\pi\nu_x/L : \nu_x \in \mathbb{Z}, 2\pi/L \leqslant |q| \leqslant 2\pi/a\}$.[18] As usual, the Fourier transform of the above functions are defined as:

$$\bar{u}(q) = \frac{1}{L}\int u_x(x)\mathbf{e}^{-iq\cdot x}dx \tag{26a}$$

$$\bar{w}(q) = \frac{1}{L}\int w(x)\mathbf{e}^{-iq\cdot x}dx \tag{26b}$$

$$\bar{A}(q) = \frac{1}{L}\int \left(\frac{\partial w}{\partial x}\right)^2 \mathbf{e}^{-iq\cdot x}dx \tag{26c}$$

Substituting the above expressions into the elastic energy formulation in Eq. (24) results in (see Appendix B for details):

$$\begin{aligned} U_b &= \frac{L^2\kappa_b}{2}\sum_{q\in\mathcal{K}_1} q^4|\bar{w}(q)|^2 \\ U_s &= \frac{L^2\bar{E}}{2}\sum_{q\in\mathcal{K}_1}\left\{\left(q\bar{u}^{\mathrm{Re}}(q) + \frac{1}{2}\bar{A}^{\mathrm{Im}}(q)\right)^2 + \left(q\bar{u}^{\mathrm{Im}}(q) - \frac{1}{2}\bar{A}^{\mathrm{Re}}(q)\right)^2 + \varepsilon_0 q^2|\bar{w}(q)|^2\right\} + \frac{L^2\bar{E}\varepsilon_0^2}{2} \end{aligned} \tag{27}$$

where the superscripts "Re" and "Im" refer to the real and imaginary parts of the functions. The partition function defined in Eq. (12) can be evaluated by integration over all possible set of displacement fields that represent *all* the possible energetic states. To represent this, the partition function is written as (Kittel, 2004):

$$Z = \int \mathrm{e}^{-\beta U}\mathcal{D}[u_x, w], \tag{28}$$

where $\beta = 1/k_BT$, and $\mathcal{D}[u_x, w]$ indicates that the integration must be carried out over all possible values of $u_x$ and $w$.

We now make an important observation which will be used later in the 2D analysis also. The total elastic energy in Eq. (24) is anharmonic with respect to $w$ but harmonic in terms of $u_x$. The partition function integration cannot be easily handled over $w$, but may be evaluated with respect to $u_x$. Integrating over $u_x$ we obtain:

$$\begin{aligned} Z &= \prod_{q\in\mathcal{K}_1}\int_{-\infty}^{\infty}\exp\left(-\beta(U_b+U_s)\right)d\bar{w}(q)d\bar{u}^{\mathrm{Re}}(q)d\bar{u}^{\mathrm{Im}}(q) \\ &= \prod_{q\in\mathcal{K}_1}\int \alpha(q)\exp(-\beta(U_b+U_s^{\mathrm{eff}}))d\bar{w}(q) \end{aligned} \tag{29}$$

wherein we have introduced the so-called *effective* strain energy which includes the remaining terms in the exponent after integrating out $u_x$. Also $\alpha(q)$ is a coefficient, independent of $w$. Using Gaussian integrals (see Appendix A) we obtain:

$$\alpha(q) = \frac{2\pi}{\beta L^2\bar{E}q^2}, \qquad U_s^{\mathrm{eff}} = \frac{L^2\bar{E}\varepsilon_0}{2}\left(\varepsilon_0 + \sum_{q\in\mathcal{K}_1} q^2|\bar{w}(q)|^2\right)$$

Consequently, the partition function integration in Eq. (29) can be evaluated to be:

$$Z = \exp\left(-\frac{\beta\bar{E}L^2\varepsilon_0^2}{2}\right)\prod_{q\in\mathcal{K}_1}\int_{-\infty}^{\infty}\frac{2\pi}{\beta L^2\bar{E}q^2}\exp\left(-\frac{L^2\beta}{2}(\kappa_b q^4 + \bar{E}\varepsilon_0 q^2)|\bar{w}(q)|^2\right)d\bar{w}(q)$$

[18] Here $a$ again, refers to the shortest possible wave-length and is in the order of the inter-atomic distances.

$$= \exp\left(-\frac{\beta\overline{E}L^2\varepsilon_0^2}{2}\right)\prod_{q\in\mathcal{K}_1}\frac{1}{L^3\overline{E}q^3}\sqrt{\frac{(2\pi)^3}{\beta^3(\overline{E}\varepsilon_0+\kappa_b q^2)}} \tag{30}$$

which, despite the anharmonic term in the elastic energy formulation in Eq. (24), can be calculated exactly. In other words, for the case of one dimensional deformation, the total energy (after integrating out $u_x$) becomes harmonic with respect to the out-of-plane displacement, and the in-plane and out-of-plane modes are *effectively* decoupled. As a result, the equipartition theorem can be applied here to obtain:

$$\langle|\overline{w}(q)|^2\rangle = \frac{k_BT}{L^2(\kappa_b q^4+\overline{E}\varepsilon_0 q^2)} \tag{31}$$

Substituting $\overline{E}=E/(1-\nu^2)$, we obtain a similar[19] expression as in the harmonic approximation (Eq. (19)) for a 2D sheet. In the following section, we extend our model to the actual two-dimensional problem of a nonlinear solid membrane.

## 5. Set-up of the statistical mechanics problem in 2D

We now return to the statistical mechanics of 2D elastic sheets predicated on the fully coupled and nonlinear energy formulation in Eq. (11). Furthermore, to eventually also assess the effect of pre-strain, we generalize our analysis to incorporate a uniform pre-existing biaxial strain $\varepsilon_0$. The nonlinear strain components are therefore:

$$\begin{aligned}
\mathcal{E}_{xx} &= \frac{\partial u_x}{\partial x}+\frac{1}{2}\left(\frac{\partial w}{\partial x}\right)^2+\varepsilon_0\\
\mathcal{E}_{yy} &= \frac{\partial u_y}{\partial y}+\frac{1}{2}\left(\frac{\partial w}{\partial y}\right)^2+\varepsilon_0\\
\mathcal{E}_{xy} &= \frac{1}{2}\left(\frac{\partial u_x}{\partial y}+\frac{\partial u_y}{\partial x}+\frac{\partial w}{\partial x}\frac{\partial w}{\partial y}\right)
\end{aligned} \tag{32}$$

As in the preceding section, we begin by expanding the displacement field in Fourier space:

$$\mathbf{u}(\mathbf{x}) = \sum_{\mathbf{q}\in\mathcal{K}}\overline{\mathbf{u}}(\mathbf{q})\mathbf{e}^{i\mathbf{q}\cdot\mathbf{x}} \tag{33a}$$

$$w(\mathbf{x}) = \sum_{\mathbf{q}\in\mathcal{K}}\overline{w}(\mathbf{q})\mathbf{e}^{i\mathbf{q}\cdot\mathbf{x}} \tag{33b}$$

$$\frac{\partial w(\mathbf{x})}{\partial x_\gamma}\frac{\partial w(\mathbf{x})}{\partial x_\delta} = \sum_{\mathbf{q}\in\mathcal{K}}\overline{A}_{\gamma\delta}(\mathbf{q})\mathbf{e}^{i\mathbf{q}\cdot\mathbf{x}} \tag{33c}$$

where $\mathcal{K}:=\{\mathbf{q}=2\pi(\nu_x,\nu_y)/L:\nu_x,\nu_y\in\mathbb{Z},|\mathbf{q}|\geqslant 2\pi/L\}$ and $\gamma$, $\delta$ denote $x$, $y$. Also, $\mathbf{u}(\mathbf{x})=(u_x(\mathbf{x}),u_y(\mathbf{x}))$.[20] The Fourier transforms of the displacement fields are:

$$\overline{\mathbf{u}}(\mathbf{q}) = \frac{1}{L^2}\int_{\mathbb{S}}\mathbf{u}(\mathbf{x})\mathbf{e}^{-i\mathbf{q}\cdot\mathbf{x}}d\mathbf{x} \tag{34a}$$

$$\overline{w}(\mathbf{q}) = \frac{1}{L^2}\int_{\mathbb{S}}w(\mathbf{x})\mathbf{e}^{-i\mathbf{q}\cdot\mathbf{x}}d\mathbf{x} \tag{34b}$$

$$\overline{A}_{\gamma\delta}(\mathbf{q}) = \frac{1}{L^2}\int_{\mathbb{S}}\frac{\partial w(\mathbf{x})}{\partial x_\gamma}\frac{\partial w(\mathbf{x})}{\partial x_\delta}\mathbf{e}^{-i\mathbf{q}\cdot\mathbf{x}}d\mathbf{x} \tag{34c}$$

Substituting the Fourier expansions in the expression for $U_{\rm h}$, $U_{\rm ac}$, and $U_{\rm anh}$, yields the following:

$$\begin{aligned}
\int U_{\rm h}d\mathbf{x} = \frac{L^2}{2}\sum_{\mathbf{q}\in\mathcal{K}}&\kappa_b\mathbf{q}^4|\overline{w}(\mathbf{q})|^2+\frac{E}{1-\nu^2}\left(\mathbf{q}^2|\overline{\mathbf{u}}(\mathbf{q})|^2+2\nu q_x\overline{u}_x(\mathbf{q})q_y\overline{u}_y(\mathbf{q})\right)\\
&+\frac{E}{1+\nu}\left(q_y^2|\overline{u}_x(\mathbf{q})|^2+q_x^2|\overline{u}_y(\mathbf{q})|^2-2q_xq_y\overline{u}_x(\mathbf{q})\overline{u}_y(-\mathbf{q})\right)+\frac{E\varepsilon_0}{2(1-\nu)}\mathbf{q}^2|\overline{w}(\mathbf{q})|^2+\frac{E\varepsilon_0^2}{1-\nu}
\end{aligned}$$

[19] Note that the 1D fluctuations in the presence of pre-strain term $\varepsilon_0$, are not exactly the same as the 2D harmonic approximation. The coefficients of $q^2$ are the well-known plane-strain, $E/(1-\nu^2)$ and biaxial modulus, $E/(1-\nu)$, corresponding to the two types of pre-strain. This is due to the Poisson effect arising from pre-straining in two directions.

[20] Similarly, $\overline{\mathbf{u}}(\mathbf{q})=(\overline{u}_x(\mathbf{q}),\overline{u}_y(\mathbf{q}))$.

$$= \frac{L^2 E \varepsilon_0^2}{2(1-\nu)} + \frac{L^2}{2}\sum_{\mathbf{q}\in\mathcal{K}} \overline{U}_{\mathrm{h}}(\mathbf{q}) \tag{35a}$$

$$\begin{aligned}\int U_{\mathrm{ac}} d\mathbf{x} &= \frac{L^2}{2}\sum_{\mathbf{q}\in\mathcal{K}} \frac{E}{1-\nu^2}\Big\{\overline{A}_{xx}^{\mathrm{Re}}(\mathbf{q})(q_x\overline{u}_x^{\mathrm{Im}}(\mathbf{q}) + \nu q_y \overline{u}_y^{\mathrm{Im}}(\mathbf{q})) + \overline{A}_{yy}^{\mathrm{Re}}(\mathbf{q})(q_y\overline{u}_y^{\mathrm{Im}}(\mathbf{q}) + \nu q_x \overline{u}_x^{\mathrm{Im}}(\mathbf{q})) \\ &\quad - \overline{A}_{xx}^{\mathrm{Im}}(\mathbf{q})(q_x\overline{u}_x^{\mathrm{Re}}(\mathbf{q}) + \nu q_y \overline{u}_y^{\mathrm{Re}}(\mathbf{q})) - \overline{A}_{yy}^{\mathrm{Im}}(\mathbf{q})(q_y\overline{u}_y^{\mathrm{Re}}(\mathbf{q}) + \nu q_x \overline{u}_x^{\mathrm{Re}}(\mathbf{q}))\Big\} \\ &\quad + \frac{E}{1+\nu}\Big\{\overline{A}_{xy}^{\mathrm{Re}}(\mathbf{q})(q_y\overline{u}_x^{\mathrm{Im}}(\mathbf{q}) + q_x \overline{u}_y^{\mathrm{Im}}(\mathbf{q})) - \overline{A}_{xy}^{\mathrm{Im}}(\mathbf{q})(q_y\overline{u}_x^{\mathrm{Re}}(\mathbf{q}) + q_x \overline{u}_y^{\mathrm{Re}}(\mathbf{q}))\Big\} \\ &= \frac{L^2}{2}\sum_{\mathbf{q}\in\mathcal{K}} \overline{U}_{\mathrm{ac}}(\mathbf{q})\end{aligned} \tag{35b}$$

$$\begin{aligned}\int U_{\mathrm{anh}} d\mathbf{x} &= \frac{L^2}{8}\sum_{\mathbf{q}\in\mathcal{K}} \frac{E}{1-\nu^2}\left(|\overline{A}_{xx}(\mathbf{q})|^2 + |\overline{A}_{yy}(\mathbf{q})|^2 + 2|\overline{A}_{xy}(\mathbf{q})|^2\right) \\ &= \frac{L^2}{2}\sum_{\mathbf{q}\in\mathcal{K}} \overline{U}_{\mathrm{anh}}(\mathbf{q})\end{aligned} \tag{35c}$$

where we have dropped all the imaginary parts of the summations—see Appendix B for further details.

We note that the total elastic energy is harmonic with respect to the in-plane displacement field. Therefore, using the expression of the total elastic energy in Fourier space, we can proceed to integrate the partition function over the in-plane displacement field:

$$\begin{aligned}Z &= \int \exp(-\beta U)\mathcal{D}[w, \mathbf{u}] \\ &= C(\varepsilon_0)\prod_{\mathbf{q}\in\mathcal{K}}\int_{-\infty}^{\infty} \exp\left(-\frac{\beta L^2}{2}\sum_{\mathbf{q}\in\mathcal{K}}(\overline{U}_{\mathrm{h}}(\mathbf{q}) + \overline{U}_{\mathrm{ac}}(\mathbf{q}) + \overline{U}_{\mathrm{anh}}(\mathbf{q}))\right) d\overline{w}(\mathbf{q}) d\overline{u}_x^{\mathrm{Re}}(\mathbf{q}) d\overline{u}_x^{\mathrm{Im}}(\mathbf{q}) d\overline{u}_y^{\mathrm{Re}}(\mathbf{q}) d\overline{u}_y^{\mathrm{Im}}(\mathbf{q}) \\ &= C(\varepsilon_0)\prod_{\mathbf{q}\in\mathcal{K}}\int \alpha(\mathbf{q}) \exp(-\beta(U_b + U_s^{\mathrm{eff}})) d\overline{w}(\mathbf{q})\end{aligned} \tag{36}$$

where $C(\varepsilon_0) = \exp(-\frac{\beta L^2 E \varepsilon_0^2}{2(1-\nu)})$. Here, the Gaussian integrals as summarized in Appendix A have been used to integrate with respect to the in-plane displacement components. As a result, the remaining terms in the exponent can be expressed in terms of an "effective strain energy" which is solely a function of the out-of-plane displacement.[21] Analogous to the 1D case described in the previous section, the effective strain energy, that consists of the remainder terms once the in-plane terms have been integrated out, can be expressed as:

$$U_s^{\mathrm{eff}} = \frac{E\varepsilon_0}{2(1-\nu)} L^2 \sum_{\mathbf{q}\in\mathcal{K}} \mathbf{q}^2 |\overline{w}(\mathbf{q})|^2 + \frac{1}{8} E L^2 \sum_{\mathbf{q}\in\mathcal{K}} \Psi(\mathbf{q})\Psi^*(\mathbf{q}) \tag{37}$$

in which, for ease of notation, we have defined $\Psi(\mathbf{q})$ as:

$$\Psi(\mathbf{q}) = \frac{1}{\mathbf{q}^2}\left\{q_y^2 \overline{A}_{xx}(\mathbf{q}) + q_x^2 \overline{A}_{yy}(\mathbf{q}) - 2q_x q_y \overline{A}_{xy}(\mathbf{q})\right\} \tag{38}$$

[21] Also, $\alpha(\mathbf{q})$ is obtained as: $\alpha(\mathbf{q}) = 2(1-\nu)(1+\nu)^2\left(\frac{\pi k_B T}{E L^2 |\mathbf{q}|^2}\right)^2$.

Furthermore, we can more compactly express the strain energy using the so-called transverse projector operator (Nelson et al., 2004) as below[22]:

$$\Psi(\mathbf{q}) = P_{ij}^{T}(\mathbf{q})\overline{A}_{ij}(\mathbf{q}) \tag{39}$$

in which

$$P_{ij}^{T}(\mathbf{q}) = \delta_{ij} - \frac{q_i q_j}{\mathbf{q}^2} \tag{40}$$

Accordingly, the total effective elastic energy in Fourier space can be written as:

$$\begin{aligned} U^{\text{eff}} &= U_b + U_s^{\text{eff}} \\ &= \frac{1}{2}\kappa_b L^2 \sum_{\mathbf{q}\in\mathcal{K}} \mathbf{q}^4 |w(\mathbf{q})|^2 + \frac{E\varepsilon_0}{2(1-\nu)} L^2 \sum_{\mathbf{q}\in\mathcal{K}} \mathbf{q}^2 |\overline{w}(\mathbf{q})|^2 + \frac{1}{2} EL^2 \sum_{\mathbf{q}\in\mathcal{K}} |\frac{1}{2} P_{ij}^{T}(\mathbf{q}) A_{ij}(\mathbf{q})|^2 \end{aligned} \tag{41}$$

The derivation up to this point has essentially decoupled the in-plane and out of plane displacement and we are now left with a nonlinear statistical mechanics problem embodied by $U^{\text{eff}}$ which is a function only of the out-of-plane displacement $w$.

## 6. Thermal fluctuations and effective bending stiffness

In this section we study the fluctuations of the out-of-plane displacement field and derive the effective bending stiffness of a solid membrane—using the effective energy in Eq. (41) as the starting point. The underlying idea is that the effects of nonlinearities can be buried in a so-called *renormalized* bending stiffness which can be then employed in a harmonic energy form. In the following, we further elaborate on this notion. Consider a nonlinear energy functional $\mathcal{H}$. Let $\mathcal{H}_0$ and $\mathcal{H}_p$ be the harmonic and anharmonic parts of the total energy $\mathcal{H}$, respectively. Then the effective bending stiffness in its general (mode-dependent) form is defined via:

$$\mathcal{H} = \mathcal{H}_0 + \mathcal{H}_p := L^2 \sum_{\mathbf{k}\in\mathcal{K}} \frac{1}{2} \kappa^{\text{eff}}(\mathbf{k}) \mathbf{k}^4 |\overline{w}(\mathbf{k})|^2 \tag{42}$$

where we introduced $\mathbf{k}$ dependency for the effective rigidity, $\kappa^{\text{eff}}(\mathbf{k})$. We remark that within a linearized (harmonic) formulation, the bending rigidity $\kappa_b$, is constant for all fluctuation modes and results in a $1/|\mathbf{k}|^4$ dependence of the out-of-plane undulations. However, in the presence of pre-strain or the nonlinear in-plane strain, the fluctuations can be described more generally as:

$$\langle |\overline{w}(\mathbf{k})|^2 \rangle \sim \left( \sum_i \alpha_i |\mathbf{k}|^{\xi_i} \right)^{-1} = \frac{1}{\alpha_1 |\mathbf{k}|^{\xi_1} + \alpha_2 |\mathbf{k}|^{\xi_2} + \alpha_3 |\mathbf{k}|^{\xi_3} + \alpha_4 |\mathbf{k}|^{\xi_4} + \cdots} \tag{43}$$

where $\xi_i$ are not necessarily integers. In this case, the dominant modes of the fluctuations are the long wave-length modes, where $\mathbf{k} \to 0$. Therefore, the term with smaller exponents $\xi_i$ in the denominator of Eq. (43) will be the leading term in the summation. Accordingly, we can *approximately* describe the fluctuations in terms of the leading term as: $\langle \overline{w}(\mathbf{k})^2 \rangle \sim 1/\mathbf{k}^{\xi}$, with $\xi$ being the smallest exponent in the denominator of Eq. (43). In this manner, the effective bending stiffness varies with the fluctuation mode as: $\kappa^{\text{eff}}(\mathbf{k}) \sim \mathbf{k}^{\xi-4}$. Henceforth, we set $\zeta = 4 - \xi \geqslant 0$ and our goal is to obtain an estimate of $\zeta$.

We first start with the naive perturbation approach in the following section. Subsequently, we attempt to improve our results by using a variational approach.

### 6.1. Regular perturbation approximation

Consider the nonlinear Hamiltonian in Eq. (42). The idea is that the nonlinear part is a small perturbation compared to the quadratic functional $\mathcal{H}_0$. Let $F$, be the free energy of the system. In the absence of the nonlinear perturbation term $\mathcal{H}_p$, the partition function $Z_0$ and free energy $F_0$ can be easily obtained using standard Gaussian integrations. The effect of the

[22] Note that $\Psi(\mathbf{q})\Psi^*(\mathbf{q}) = \Psi(\mathbf{q})\Psi(-\mathbf{q}) = |\Psi(\mathbf{q})|^2$ and is expanded as follows:

$$\begin{aligned} \Psi(\mathbf{q})\Psi(-\mathbf{q}) &= |\Psi(\mathbf{q})|^2 \\ &= \frac{1}{(q_x^2+q_y^2)^2} \Big\{ q_x^4 \overline{A}_{yy}^{\text{Re}}(\mathbf{q})^2 + q_x^4 \overline{A}_{yy}^{\text{Im}}(\mathbf{q})^2 + q_y^4 \overline{A}_{xx}^{\text{Re}}(\mathbf{q})^2 + q_y^4 \overline{A}_{xx}^{\text{Im}}(\mathbf{q})^2 - 4q_x q_y^3 \overline{A}_{xx}^{\text{Im}}(\mathbf{q}) \overline{A}_{xy}^{\text{Im}}(\mathbf{q}) \\ &\quad + 2q_x^2 q_y^2 \overline{A}_{xx}^{\text{Im}}(\mathbf{q}) \overline{A}_{yy}^{\text{Im}}(\mathbf{q}) - 4q_x^3 q_y \overline{A}_{xy}^{\text{Im}}(\mathbf{q}) \overline{A}_{yy}^{\text{Im}}(\mathbf{q}) + 4q_x^2 q_y^2 \overline{A}_{xy}^{\text{Im}}(\mathbf{q})^2 + q_x^4 \overline{A}_{yy}^{\text{Im}}(\mathbf{q})^2 + q_y^4 \overline{A}_{xx}^{\text{Im}}(\mathbf{q})^2 \\ &\quad - 4q_x q_y^3 \overline{A}_{xx}^{\text{Re}}(\mathbf{q}) \overline{A}_{xy}^{\text{Re}}(\mathbf{q}) + 2q_x^2 q_y^2 \overline{A}_{xx}^{\text{Re}}(\mathbf{q}) \overline{A}_{yy}^{\text{Re}}(\mathbf{q}) - 4q_x^3 q_y \overline{A}_{xy}^{\text{Re}}(\mathbf{q}) \overline{A}_{yy}^{\text{Re}}(\mathbf{q}) + 4q_x^2 q_y^2 \overline{A}_{xy}^{\text{Re}}(\mathbf{q})^2 \Big\}. \end{aligned}$$

nonlinear term on the total free energy of the system, can be then estimated by a perturbation expansion around $F_0$. We start with expanding the partition function of the system $Z$:

$$Z = \int \exp(-\beta(\mathcal{H}_0 + \mathcal{H}_p))\mathcal{D}[w] = Z_0\langle \exp(-\beta\mathcal{H}_p)\rangle_{\mathcal{H}_0} \tag{44}$$

wherein the subscript $\langle\cdot\rangle_{\mathcal{H}_0}$ denotes ensemble average with respect to $\mathcal{H}_0$. The exponential term in the above equation can be expanded in a Taylor series as:

$$\exp(-\beta\mathcal{H}_p) = 1 - \beta\mathcal{H}_p + \frac{1}{2}(\beta\mathcal{H}_p)^2 + \cdots = \sum_{n=0}^{\infty}\frac{(-\beta\mathcal{H}_p)^n}{n!} \tag{45}$$

Then the free energy of the system is obtained as:

$$F = -\frac{1}{\beta}\log Z = F_0 - \frac{1}{\beta}\log(1 + \sum_{n=1}^{\infty}\frac{\langle(-\beta\mathcal{H}_p)^n\rangle_{\mathcal{H}_0}}{n!}) \tag{46}$$

Expanding the logarithm term we have:

$$\log\left(\sum_{n=0}^{\infty}\frac{(-\beta)^n\langle\mathcal{H}_p^n\rangle_{\mathcal{H}_0}}{n!}\right) = \left(\sum_{n=1}^{\infty}\frac{(-\beta)^n\langle\mathcal{H}_p^n\rangle_{\mathcal{H}_0}}{n!}\right) - \frac{1}{2}\left(\sum_{n=1}\frac{(-\beta)^n\langle\mathcal{H}_p^n\rangle_{\mathcal{H}_0}}{n!}\right)^2 + \cdots \tag{47}$$

and hence, the free energy expansion can be derived to be:

$$F = F_0 - \frac{1}{\beta}\sum_{n=1}^{\infty}\frac{(-\beta)^n}{n!}\langle\mathcal{H}_p^n\rangle_{\mathcal{H}_0}^c \tag{48}$$

where the superscript $\langle\cdot\rangle^c$ denotes the cumulant averages.[23]The infinite series in the above equation gives us the exact average amount of energy that the nonlinear term adds to the system. In practice, however, we need to truncate the series to some finite order. If the nonlinear term is small and the series is well-behaved we can expect to achieve a reasonable estimate by evaluating the first few terms of perturbation expansion in Eq. (48). In what follows, we use this notion to obtain an estimate of the excess energy that is added to the system due to nonlinearity. The excess free energy can be then captured in terms of the effective bending stiffness. The average energy of the system with the nonlinear Hamiltonian in Eq. (41) is (up to a first order):

$$\begin{aligned}\langle\mathcal{H}\rangle &= \left\langle \frac{1}{2}\kappa_b L^2\sum_{\mathbf{k}\in\mathcal{K}}\mathbf{k}^4|\overline{w}(\mathbf{k})|^2 + \frac{E\varepsilon_0}{2(1-\nu)}L^2\sum_{\mathbf{k}\in\mathcal{K}}\mathbf{k}^2|\overline{w}(\mathbf{k})|^2\right\rangle_{\mathcal{H}_0} + \left\langle \frac{1}{2}EL^2\sum_{\mathbf{q}\in\mathcal{K}}|\frac{1}{2}P_{ij}^T(\mathbf{q})\overline{A}_{ij}(\mathbf{q})|^2\right\rangle_{\mathcal{H}_0}\\ &:= \frac{L^2}{2}\sum_{\mathbf{k}\in\mathcal{K}}\kappa_{\text{eff}}(\mathbf{k})\ \mathbf{k}^4\langle|\overline{w}(\mathbf{k})|^2\rangle_{\mathcal{H}_0}\end{aligned} \tag{49}$$

To calculate the averages in Eq. (49), we start by expanding the out-of-plane displacement field in Fourier space:

$$\begin{aligned}\frac{\partial w}{\partial x_i}\frac{\partial w}{\partial x_j} &= \sum_{\mathbf{k},\mathbf{k}'\in\mathcal{K}} -k_i k_j'\overline{w}(\mathbf{k})\overline{w}(\mathbf{k}')e^{i(\mathbf{k}+\mathbf{k}')\cdot\mathbf{x}}\\ &= \sum_{\mathbf{k},\mathbf{q}\in\mathcal{K}} -k_i(q_j - k_j)\overline{w}(\mathbf{k})\overline{w}(\mathbf{q}-\mathbf{k})e^{i\mathbf{q}\cdot\mathbf{x}} = \sum_{\mathbf{q}\in\mathcal{K}}\overline{A}_{ij}(\mathbf{q})e^{i\mathbf{q}\cdot\mathbf{x}}\end{aligned} \tag{50a}$$

in which:

$$\overline{A}_{ij}(\mathbf{q}) = \sum_{\mathbf{k}\in\mathcal{K}} -k_i(q_j - k_j)\overline{w}(\mathbf{k})\overline{w}(\mathbf{q}-\mathbf{k}) \tag{51}$$

[23] The cumulant averages, up to fourth order, are:

$$\begin{aligned}\langle\mathcal{H}_p\rangle_{\mathcal{H}_0}^c &= \langle\mathcal{H}_p\rangle_{\mathcal{H}_0}\\ \langle\mathcal{H}_p^2\rangle_{\mathcal{H}_0}^c &= \langle\mathcal{H}_p^2\rangle_{\mathcal{H}_0} - \langle\mathcal{H}_p\rangle_{\mathcal{H}_0}^2\\ \langle\mathcal{H}_p^3\rangle_{\mathcal{H}_0}^c &= \langle\mathcal{H}_p^3\rangle_{\mathcal{H}_0} - 3\langle\mathcal{H}_p^2\rangle_{\mathcal{H}_0}\langle\mathcal{H}_p\rangle_{\mathcal{H}_0} + 2\langle\mathcal{H}_p\rangle_{\mathcal{H}_0}^3\\ \langle\mathcal{H}_p^4\rangle_{\mathcal{H}_0}^c &= \langle\mathcal{H}_p^4\rangle_{\mathcal{H}_0} - 3\langle\mathcal{H}_p^3\rangle_{\mathcal{H}_0}\langle\mathcal{H}_p\rangle_{\mathcal{H}_0} - 3\langle\mathcal{H}_p^2\rangle_{\mathcal{H}_0}^2 + 12\langle\mathcal{H}_p^2\rangle_{\mathcal{H}_0}\langle\mathcal{H}_p\rangle_{\mathcal{H}_0}^2 - 6\langle\mathcal{H}_p\rangle_{\mathcal{H}_0}^4\end{aligned}$$

Accordingly, the excess free energy can be related to the total average energy of the system up to $n$-th order as:

$$\langle\mathcal{H}\rangle = \langle\mathcal{H}_0\rangle_{\mathcal{H}_0} + \frac{1}{\beta}\sum_{n=1}^{\infty}\frac{(-\beta)^n}{n!}\langle\mathcal{H}_p^n\rangle_{\mathcal{H}_0}^c.$$

After substituting the operator $P^T_{ij}(\mathbf{q})$, we obtain:

$$P^T_{ij}(\mathbf{q})\overline{A}_{ij}(\mathbf{q}) = \sum_{\mathbf{k}\in\mathcal{K}}\left(-k_i(q_i-k_i)+\frac{k_iq_iq_j(q_j-k_j)}{\mathbf{q}^2}\right)\overline{w}(\mathbf{k})\overline{w}(\mathbf{q}-\mathbf{k})$$
$$= \sum_{\mathbf{k}\in\mathcal{K}}\frac{\mathbf{k}^2\mathbf{q}^2-(\mathbf{k}\cdot\mathbf{q})^2}{\mathbf{q}^2}\overline{w}(\mathbf{k})\overline{w}(\mathbf{q}-\mathbf{k}) = \sum_{\mathbf{k}\in\mathcal{K}}\Omega(\mathbf{q},\mathbf{k})\overline{w}(\mathbf{k})\overline{w}(\mathbf{q}-\mathbf{k}) \tag{52}$$

where we have also introduced $\Omega(\mathbf{q}, \mathbf{k})$ for the ease of notation in subsequent calculations. The magnitude of the above expressions in each mode is then:

$$|P^T_{ij}(\mathbf{q})\overline{A}_{ij}(\mathbf{q})|^2 = \left(P^T_{ij}(\mathbf{q})\overline{A}_{ij}(\mathbf{q})\right)\times\left(P^T_{ij}(-\mathbf{q})\overline{A}_{ij}(-\mathbf{q})\right)$$
$$= \sum_{\mathbf{k},\mathbf{k}'\in\mathcal{K}}\Omega(\mathbf{q},\mathbf{k})\Omega(-\mathbf{q},\mathbf{k}')\overline{w}(\mathbf{k})\overline{w}(\mathbf{q}-\mathbf{k})\overline{w}(\mathbf{k}')\overline{w}(-\mathbf{q}-\mathbf{k}') \tag{53}$$

Now, we proceed to calculate the ensemble average of the expression in Eq. (53). We emphasize that the averaging is carried out with respect to the quadratic part of the elastic energy which is:

$$\mathcal{H}_0 = \frac{L^2}{2}\sum_{\mathbf{k}\in\mathcal{K}}(\kappa_b\mathbf{k}^4+\overline{E}\varepsilon_0\mathbf{k}^2)|\overline{w}(\mathbf{k})|^2 \tag{54}$$

We then obtain:

$$\sum_{\mathbf{q}\in\mathcal{K}}\langle|P^T_{ij}(\mathbf{q})A_{ij}(\mathbf{q})|^2\rangle_{\mathcal{H}_0} = \sum_{\mathbf{q},\mathbf{k},\mathbf{k}'\in\mathcal{K}}\Omega(\mathbf{q},\mathbf{k})\Omega(-\mathbf{q},\mathbf{k}')\left\langle\overline{w}(\mathbf{k})\overline{w}(\mathbf{q}-\mathbf{k})\overline{w}(\mathbf{k}')\overline{w}(-\mathbf{q}-\mathbf{k}')\right\rangle_{\mathcal{H}_0} \tag{55}$$

From Wick's theorem (Kleinert, 2009), the above average —with respect to the *quadratic* Hamiltonian (54)— is nonzero only when the modes $\mathbf{k}_i$ are decoupled—see Appendix C—and that is:

$$\langle\overline{w}(\mathbf{k}_1)\overline{w}(\mathbf{k}_2)\overline{w}(\mathbf{k}_3)\overline{w}(\mathbf{k}_4)\rangle_{\mathcal{H}_0} = \langle|\overline{w}(\mathbf{k}_1)|^2\rangle_{\mathcal{H}_0}\langle|\overline{w}(\mathbf{k}_2)|^2\rangle_{\mathcal{H}_0}\left\{\delta(\mathbf{k}_1,-\mathbf{k}_3)\delta(\mathbf{k}_2,-\mathbf{k}_4)+\delta(\mathbf{k}_1,-\mathbf{k}_4)\delta(\mathbf{k}_2,-\mathbf{k}_3)\right\}$$
$$+\langle|\overline{w}(\mathbf{k}_1)|^2\rangle_{\mathcal{H}_0}\langle|\overline{w}(\mathbf{k}_3)|^2\rangle_{\mathcal{H}_0}\delta(\mathbf{k}_1,-\mathbf{k}_2)\delta(\mathbf{k}_3,-\mathbf{k}_4) \tag{56}$$

Note that the case $\mathbf{k}=-\mathbf{q}+\mathbf{k}$ is true only in zeroth mode when $\mathbf{q}\to 0$. The only nonzero case for all modes is when $\mathbf{k}=-\mathbf{k}'$. Hence, the summation in Eq. (55) can be obtained as:

$$\sum_{\mathbf{q}\in\mathcal{K}}\langle|P^T_{ij}(\mathbf{q})\overline{A}_{ij}(\mathbf{q})|^2\rangle_{\mathcal{H}_0} = \sum_{\mathbf{q},\mathbf{k}\in\mathcal{K}}\Omega(\mathbf{q},\mathbf{k})^2\langle|\overline{w}(\mathbf{k})|^2\rangle_{\mathcal{H}_0}\langle|\overline{w}(\mathbf{q}-\mathbf{k})|^2\rangle_{\mathcal{H}_0} \tag{57}$$

Substituting the averages of the quadratic term in Eq. (54) as well as the non-quadratic part in Eq. (57) into Eq. (49), we can obtain a first order estimate of the effective stiffness:

$$\langle\mathcal{H}\rangle = \frac{L^2}{2}\sum_{\mathbf{k}\in\mathcal{K}}\left(\kappa_b\mathbf{k}^4+\frac{E\varepsilon_0}{(1-\nu)}\mathbf{k}^2+\frac{E}{4}\sum_{\mathbf{q}\in\mathcal{K}}\Omega(\mathbf{q},\mathbf{k})^2\langle|\overline{w}(\mathbf{q}-\mathbf{k})|^2\rangle_{\mathcal{H}_0}\right)\langle|\overline{w}(\mathbf{k})|^2\rangle_{\mathcal{H}_0}$$
$$:= \frac{L^2}{2}\sum_{\mathbf{k}\in\mathcal{K}}\kappa^{\text{eff}}(\mathbf{k})\mathbf{k}^4\langle|\overline{w}(\mathbf{k})|^2\rangle_{\mathcal{H}_0} \tag{58}$$

The ensemble average $\langle|\overline{w}(\mathbf{q}-\mathbf{k})|^2\rangle_{\mathcal{H}_0}$ should be carried out with respect to the harmonic part of the total energy:

$$\langle|\overline{w}(\mathbf{q}-\mathbf{k})|^2\rangle_{\mathcal{H}_0} = \frac{k_BT}{L^2(\kappa_b|\mathbf{q}-\mathbf{k}|^4+\overline{E}\varepsilon_0|\mathbf{q}-\mathbf{k}|^2)} \tag{59}$$

from which, the effective stiffness may be evaluated to be:

$$\kappa^{\text{eff}}(\mathbf{k}) = \kappa_b+\frac{E\varepsilon_0}{(1-\nu)|k|^2}+\frac{1}{4}k_BTE\sum_{\mathbf{q}\in\mathcal{K}}\frac{\Omega(\mathbf{q},\mathbf{k})^2}{L^2|\mathbf{k}|^4(\kappa_b|\mathbf{q}-\mathbf{k}|^4+\overline{E}\varepsilon_0|\mathbf{q}-\mathbf{k}|^2)} \tag{60}$$

In the remainder of this section, we analyze the expression in Eq. (60) for the two cases of zero and non-zero pre-strain field $\varepsilon_0$.

*6.1.1. Case I: $\varepsilon_0 = 0$*

When the in-plane pre-strain term is zero, the expression for the effective bending stiffness in Eq. (60) reduces to:

$$\kappa^{\text{eff}}(\mathbf{k}) = \kappa_b+\frac{k_BTE}{4\kappa_b}\sum_{\mathbf{q}\in\mathcal{K}}\frac{\Omega(\mathbf{q},\mathbf{k})^2}{L^2|\mathbf{k}|^4|\mathbf{q}-\mathbf{k}|^4} \tag{61}$$

Our goal is to find the dominant factor in Eq. (61). To this end, we seek the $\mathbf{k}$ dependency of the second term in Eq. (61). In the long wave-length limit as $\mathbf{k}\to 0-$ which is the leading mode in the summation, the numerator varies as $(\mathbf{k}^2\mathbf{q}^2-(\mathbf{k}\cdot\mathbf{q})^2)^2\sim\mathbf{k}^4\mathbf{q}^4$ and hence, the whole term varies as:

$$\frac{(\mathbf{k}^2\mathbf{q}^2-(\mathbf{k}\cdot\mathbf{q})^2)^2}{|\mathbf{q}-\mathbf{k}|^4|\mathbf{q}|^4|\mathbf{k}|^4}\sim\frac{1}{|\mathbf{q}-\mathbf{k}|^4} \tag{62}$$

and consequently, when the summation is carried out over $\mathbf{q}$.[24] the resulting leading order term is obtained as: $\sum_{\mathbf{q}\in\mathcal{K}}|\mathbf{q}-\mathbf{k}|^{-4}\sim|\mathbf{k}|^{-2}$. Therefore, the effective stiffness for this case can be written as:

$$\kappa^{\text{eff}}(\mathbf{k})=\kappa_b+\frac{\alpha' k_BTE}{\kappa_b|\mathbf{k}|^2} \tag{63}$$

where $\alpha'$ is the correction factor. The long wave-length fluctuations is then obtained as:

$$\langle|w(\mathbf{k})|^2\rangle=\frac{k_BT}{L^2\kappa^{\text{eff}}(\mathbf{k})|\mathbf{k}|^4}\sim\frac{k_BT}{L^2(\kappa_b|\mathbf{k}|^4+\alpha' k_BTE|\mathbf{k}|^2/\kappa_b)} \tag{64}$$

and hence in real space, the fluctuations scale as:

$$\begin{aligned}\langle w^2\rangle&\sim\frac{\kappa_b k_BT}{4\pi\alpha' E}\log\left(1+\frac{\alpha' k_BTEL^2}{4\pi^2\kappa_b^2}\right)\\&\sim\frac{k_BTL^2}{16\pi^3\kappa_b}-\frac{k_BTEL^4}{128\pi^5\kappa_b^3}\alpha'+\cdots+\mathcal{O}(\alpha'^2)\end{aligned} \tag{65}$$

We remark that up to a first order, the real space fluctuations in this case are similar to what we obtained earlier in Eq. (22) for the harmonic approximation with a pre-strain term.

The results in Eqs. (63) and (65) are first order estimates from perturbation expansion and may be reasonable at low temperatures.

#### 6.1.2. Case II: $\varepsilon_0\neq 0$

Using similar scaling arguments as before, we seek the $\mathbf{k}$ dependency of the last term in Eq. (60). In the long wave-length limit as $\mathbf{k}\to 0-$ which is the dominant mode in the summation, the numerator varies as $(\mathbf{k}^2\mathbf{q}^2-(\mathbf{k}\cdot\mathbf{q})^2)^2\sim\mathbf{k}^4\mathbf{q}^4$, while the denominator varies as: $\big(\kappa_b|\mathbf{q}-\mathbf{k}|^4+E\varepsilon_0|\mathbf{q}-\mathbf{k}|^2/(1-\nu)\big)|\mathbf{q}|^4|\mathbf{k}|^4\sim|\mathbf{q}|^4|\mathbf{k}|^4E\varepsilon_0|\mathbf{q}-\mathbf{k}|^2/(1-\nu)$. Thus, the dominant term of the whole fraction in the summation is proportional to:

$$\frac{(\mathbf{k}^2\mathbf{q}^2-(\mathbf{k}\cdot\mathbf{q})^2)^2}{\big(\kappa_b|\mathbf{q}-\mathbf{k}|^4+E\varepsilon_0|\mathbf{q}-\mathbf{k}|^2/(1-\nu)\big)|\mathbf{q}|^4|\mathbf{k}|^4}\sim\frac{1}{E\varepsilon_0|\mathbf{q}-\mathbf{k}|^2/(1-\nu)} \tag{66}$$

Carrying out the summation of the expression in Eq. (66) over $\mathbf{q}$, results in a constant that is independent of $\mathbf{k}$. Accordingly, the dominant term in Eq. (60) will be $E\varepsilon_0/\mathbf{k}^2$ and the effective stiffness can be expressed as:

$$\kappa^{\text{eff}}(\mathbf{k})\sim\kappa_b+\frac{E\varepsilon_0}{(1-\nu)\mathbf{k}^2}+\text{Const.} \tag{67}$$

from which the fluctuations scale as:

$$\langle w^2\rangle\sim\frac{k_BT}{4\pi\bar{E}\varepsilon_0}\log\left(1+\frac{\bar{E}\varepsilon_0L^2}{4\pi^2(\kappa_b+\alpha)}\right) \tag{68}$$

where $\alpha$ is the constant in Eq. (67). We note that the above result is *qualitatively* the same as what is obtained using the linearized energy formulation in Eq. (21). In the next section we improve our estimate of the effective bending stiffness and out-of-plane fluctuations by using a variational perturbation theory.

### 6.2. Variational perturbation theory (VPT)

To improve the results of what can be obtained from what we have termed as the naive perturbation approach (preceding section), we adopt an alternative version of it that is rooted in a variational argument. The key idea was first introduced by Kleinert (2009) in the context of anharmonic Hamiltonians arising in quantum mechanics. We briefly elaborate on the details of the procedure keeping in mind the intended audience of this work. We start with adding and subtracting a trial Hamiltonian to the nonlinear energy formulation in Eq. (41). In order to describe the out-of-plane fluctuations, consider a trial Hamiltonian as:

$$\mathcal{H}_{\text{trial}}=\frac{1}{2}L^2\sum_{\mathbf{k}\in\mathcal{K}}\kappa^{\text{eff}}(\mathbf{k})\mathbf{k}^4|w(\mathbf{k})|^2 \tag{69}$$

[24] The summation can be carried out using a double integration, or alternatively in polar coordinate with varying radius of $q=|\mathbf{q}|$.

where $\kappa^{\text{eff}}$ is the unknown effective bending stiffness in general mode-dependent form. Then the total elastic energy can be written as:

$$U_b + U_s^{\text{eff}} = \mathcal{H}_{\text{trial}} + (U_b + U_s^{\text{eff}} - \mathcal{H}_{\text{trial}}) \tag{70}$$

The perturbation expansion of the free energy associated with the Hamiltonian in Eq. (70) is obtained by the Taylor series in Eq. (48):

$$F_\infty = F_0 - \frac{1}{\beta}\sum_{N=1}^{\infty}\frac{(-\beta)^N}{N!}\langle\left[U_b + U_s^{\text{eff}} - \mathcal{H}_{\text{trial}}\right]^N\rangle_{\mathcal{H}_{\text{trial}}}^{c} \tag{71}$$

where $F_0$ is the free energy corresponding to the trial Hamiltonian $\mathcal{H}_{\text{trial}}$:

$$\begin{aligned} F_0 &= \sum_{\mathbf{k}\in\mathcal{K}}\frac{1}{2\beta}\left(\log(\frac{L^2|\mathbf{k}|^4}{2\pi}) + \log(\beta\kappa^{\text{eff}}(\mathbf{k}))\right) \\ &= C_F + \sum_{\mathbf{k}\in\mathcal{K}}\frac{1}{2\beta}\log(\beta\kappa^{\text{eff}}(\mathbf{k})) \end{aligned} \tag{72}$$

where we have labeled the first term $C_F$—a term that is independent of the effective stiffness $\kappa^{\text{eff}}(\mathbf{k})$. Needless to say that the full expansion in Eq. (71) as $N\to\infty$ *should be* independent of the choice of the trial Hamiltonian. In practice, however, the series is truncated up to a finite order $M$ to obtain an estimate of the free energy. Unlike the infinite series expansion in Eq. (71), the truncated series $F_M$ *does* depend on the choice of the trial Hamiltonian $\mathcal{H}_{\text{trial}}$. Accordingly, in order to obtain an optimized estimate, we need to minimize the *sensitivity* of the truncated series to the trial Hamiltonian. To this end, we set (Kleinert, 2009):

$$\frac{\partial F_M}{\partial\kappa^{\text{eff}}(\mathbf{k})} := 0. \tag{73}$$

In a rather good approximation, the result for the truncated series of the variational free energy from this method will converge i.e. $F_M \approx F_{M+1}$ and exhibit minimal sensitivity to the trial function. We remark that restricting calculations to first order in the truncated series yields just the well-known *Bogoliubov theorem* (Safran, 1994) for the upper bound of the exact free energy:

$$F_{\text{var}} \leqslant F_0 + \langle U_b + U_s^{\text{eff}} - \mathcal{H}_{\text{trial}}\rangle_{\mathcal{H}_{\text{trial}}} \tag{74}$$

In what follows, we will use this approach up to first order to obtain a closed form estimation of the effective stiffness of the system.

We proceed to calculate the expectation values in the right hand side of the Eq. (71) up to first order.

$$\langle U_b\rangle_{\mathcal{H}_{\text{trial}}} + \langle U_s^{\text{eff}}\rangle_{\mathcal{H}_{\text{trial}}} = \frac{1}{2}\kappa_b L^2\sum_{\mathbf{k}\in\mathcal{K}}\mathbf{k}^4\langle|\overline{w}(\mathbf{k})|^2\rangle_{\mathcal{H}_{\text{trial}}} + \frac{E\varepsilon_0}{2(1-\nu)}L^2\sum_{\mathbf{k}\in\mathcal{K}}\mathbf{k}^2\langle|\overline{w}(\mathbf{k})|^2\rangle_{\mathcal{H}_{\text{trial}}} + \frac{1}{2}EL^2\sum_{\mathbf{q}\in\mathcal{K}}\langle|\frac{1}{2}P_{ij}^T(\mathbf{q})\overline{A}_{ij}(\mathbf{q})|^2\rangle_{\mathcal{H}_{\text{trial}}} \tag{75}$$

The average values for the first and second terms in Eq. (75) can be obtained by equipartition theorem: $\langle|\overline{w}(\mathbf{k})|^2\rangle_{\mathcal{H}_{\text{trial}}} = \frac{1}{L^2\beta\kappa^{\text{eff}}(\mathbf{k})|\mathbf{k}|^4}$. The expectation values for the last term has been derived earlier in Eq. (57). Here we simply substitute the average values with respect to the trial Hamiltonian $\mathcal{H}_{\text{trial}}$:

$$\begin{aligned} \sum_{\mathbf{q}\in\mathcal{K}}\langle|P_{ij}^T(\mathbf{q})\overline{A}_{ij}(\mathbf{q})|^2\rangle_{\mathcal{H}_{\text{trial}}} &= \sum_{\mathbf{q},\mathbf{k}\in\mathcal{K}}\Omega(\mathbf{q},\mathbf{k})^2\langle|\overline{w}(\mathbf{k})|^2\rangle_{\mathcal{H}_{\text{trial}}}\langle|\overline{w}(\mathbf{q}-\mathbf{k})|^2\rangle_{\mathcal{H}_{\text{trial}}} \\ &= \sum_{\mathbf{q},\mathbf{k}\in\mathcal{K}}\frac{\Omega(\mathbf{q},\mathbf{k})^2}{L^4\beta^2|\mathbf{k}|^4|\mathbf{q}-\mathbf{k}|^4\kappa^{\text{eff}}(\mathbf{k})\kappa^{\text{eff}}(\mathbf{q}-\mathbf{k})} \end{aligned} \tag{76}$$

Substituting all the terms results in the following form for the variational free energy:

$$F_{\text{var}} = C_{\text{F}} + \sum_{\mathbf{k}\in\mathcal{K}}\left\{\frac{1}{2\beta}\log(\beta\kappa^{\text{eff}}(\mathbf{k})) + \frac{\kappa_b}{2\beta\kappa^{\text{eff}}(\mathbf{k})} + \frac{E\varepsilon_0}{2\beta(1-\nu)\kappa^{\text{eff}}(\mathbf{k})|\mathbf{k}|^2} + E\sum_{\mathbf{q}\in\mathcal{K}}\frac{\Omega(\mathbf{q},\mathbf{k})^2}{8\,L^2\beta^2|\mathbf{k}|^4|\mathbf{q}-\mathbf{k}|^4\kappa^{\text{eff}}(\mathbf{k})\kappa^{\text{eff}}(\mathbf{q}-\mathbf{k})}\right\} \tag{77}$$

In the next step we take the derivatives of the variational free energy in Eq. (77) with respect to the variational parameter $\kappa^{\text{eff}}(\mathbf{k})$.

$$\frac{\partial F_{\text{var}}}{\partial \kappa^{\text{eff}}(\mathbf{k})} := 0$$

$$0 := \sum_{\mathbf{k}\in\mathcal{K}} \left\{ \frac{1}{2\beta\kappa^{\text{eff}}(\mathbf{k})} - \frac{\kappa_b}{2\beta\kappa^{\text{eff}}(\mathbf{k})^2} - \frac{E\varepsilon_0}{2\beta(1-\nu)\kappa^{\text{eff}}(\mathbf{k})^2|\mathbf{k}|^2} - E\sum_{\mathbf{q}\in\mathcal{K}} \frac{\Omega(\mathbf{q},\mathbf{k})^2}{8L^2\beta^2|\mathbf{k}|^4|\mathbf{q}-\mathbf{k}|^4\kappa^{\text{eff}}(\mathbf{k})\kappa^{\text{eff}}(\mathbf{q}-\mathbf{k})} \left( \frac{1}{\kappa^{\text{eff}}(\mathbf{k})} + \frac{1}{\kappa^{\text{eff}}(\mathbf{q}-\mathbf{k})} \frac{\partial \kappa^{\text{eff}}(\mathbf{q}-\mathbf{k})}{\partial \kappa^{\text{eff}}(\mathbf{k})} \right) \right\} \tag{78}$$

As we discussed in the beginning of this section, in order to make analytical progress, we focus on the leading term in the expression for the effective stiffness. Assuming that the leading term is described as: $\kappa^{\text{eff}}(\mathbf{k}) \sim |\mathbf{k}|^{-\zeta}$ we obtain,

$$\frac{\partial \kappa^{\text{eff}}(\mathbf{q}-\mathbf{k})}{\partial \kappa^{\text{eff}}(\mathbf{k})} = \frac{\partial \kappa^{\text{eff}}(\mathbf{q}-\mathbf{k})/\partial \mathbf{k}}{\partial \kappa^{\text{eff}}(\mathbf{k})/\partial \mathbf{k}} = \frac{|\mathbf{q}-\mathbf{k}|^{-\zeta-1}}{|\mathbf{k}|^{-\zeta-1}} = \frac{\kappa^{\text{eff}}(\mathbf{q}-\mathbf{k})}{\kappa^{\text{eff}}(\mathbf{k})} \frac{|\mathbf{k}|}{|\mathbf{q}-\mathbf{k}|} \tag{79}$$

Substituting the above expression into the derivation of $F_{\text{var}}$ results in

$$\begin{aligned} \frac{\partial F_{\text{var}}}{\partial \kappa^{\text{eff}}(\mathbf{k})} &= \sum_{\mathbf{k}\in\mathcal{K}} \left\{ \frac{1}{2\beta\kappa^{\text{eff}}(\mathbf{k})} - \frac{\kappa_b}{2\beta\kappa^{\text{eff}}(\mathbf{k})^2} - \frac{E\varepsilon_0}{2\beta(1-\nu)\kappa^{\text{eff}}(\mathbf{k})^2|\mathbf{k}|^2} \right. \\ &\quad \left. - E\sum_{\mathbf{q}\in\mathcal{K}} \frac{\Omega(\mathbf{q},\mathbf{k})^2}{8L^2\beta^2|\mathbf{k}|^4|\mathbf{q}-\mathbf{k}|^4\kappa^{\text{eff}}(\mathbf{k})^2\kappa^{\text{eff}}(\mathbf{q}-\mathbf{k})} \left( 1 + \frac{|\mathbf{k}|}{|\mathbf{q}-\mathbf{k}|} \right) \right\} \\ &= 0 \end{aligned} \tag{80}$$

Solving for $\kappa^{\text{eff}}(\mathbf{k})$, results in the following implicit equation for the effective bending stiffness:

$$\kappa^{\text{eff}}(\mathbf{k}) = \kappa_b + \frac{E\varepsilon_0}{(1-\nu)|\mathbf{k}|^2} + \frac{k_BTE}{4} \sum_{\mathbf{q}\in\mathcal{K}} \frac{\Omega(\mathbf{q},\mathbf{k})^2}{L^2|\mathbf{k}|^4|\mathbf{q}-\mathbf{k}|^4\kappa^{\text{eff}}(\mathbf{q}-\mathbf{k})} \left( 1 + \frac{|\mathbf{k}|}{|\mathbf{q}-\mathbf{k}|} \right) \tag{81}$$

We again separately address the implications of Eq. (81) for the two cases of zero and non-zero pre-strain field $\varepsilon_0$.

*6.2.1. Case I: $\varepsilon_0 = 0$*

When the in-plane strain is zero, the expression for the effective bending stiffness from Eq. (81) reduces to:

$$\kappa^{\text{eff}}(\mathbf{k}) = \kappa_b + \frac{k_BTE}{4} \sum_{\mathbf{q}\in\mathcal{K}} \frac{\Omega(\mathbf{q},\mathbf{k})^2}{L^2|\mathbf{k}|^4|\mathbf{q}-\mathbf{k}|^4\kappa^{\text{eff}}(\mathbf{q}-\mathbf{k})} \left( 1 + \frac{|\mathbf{k}|}{|\mathbf{q}-\mathbf{k}|} \right) \tag{82}$$

As before we focus on long wave-length modes ($|\mathbf{q}|, |\mathbf{k}| \to 0$, since these modes are the dominant one in the fluctuation spectra. To make analytical progress, let $\kappa^{\text{eff}}(\mathbf{q}-\mathbf{k}) \sim \Theta|\mathbf{q}-\mathbf{k}|^{-\zeta}$, where $\Theta$ is an unknown constant. Then the summation in the second term of Eq. (82) scales as:

$$\begin{aligned} \sum_{\mathbf{q}\in\mathcal{K}} \frac{\Omega(\mathbf{q},\mathbf{k})^2}{|\mathbf{k}|^4|\mathbf{q}-\mathbf{k}|^4\kappa^{\text{eff}}(\mathbf{q}-\mathbf{k})} \left( 1 + \frac{|\mathbf{k}|}{|\mathbf{q}-\mathbf{k}|} \right) &= \sum_{\mathbf{q}\in\mathcal{K}} \frac{(\mathbf{k}^2\mathbf{q}^2 - (\mathbf{k}\cdot\mathbf{q})^2)^2}{|\mathbf{q}-\mathbf{k}|^4|\mathbf{k}|^4|\mathbf{q}|^4\kappa^{\text{eff}}(\mathbf{q}-\mathbf{k})} \left( 1 + \frac{|\mathbf{k}|}{|\mathbf{q}-\mathbf{k}|} \right) \\ &\sim \sum_{\mathbf{q}\in\mathcal{K}} \frac{1}{|\mathbf{q}-\mathbf{k}|^4\kappa^{\text{eff}}(\mathbf{q}-\mathbf{k})} \left( 1 + \frac{|\mathbf{k}|}{|\mathbf{q}-\mathbf{k}|} \right) \\ &\sim \sum_{\mathbf{q}\in\mathcal{K}} \frac{1}{|\mathbf{q}-\mathbf{k}|^{4-\zeta}} \left( 1 + \frac{|\mathbf{k}|}{|\mathbf{q}-\mathbf{k}|} \right) \\ &\sim \frac{1}{|\mathbf{k}|^{2-\zeta}} \end{aligned} \tag{83}$$

We note that the summation in Eq. (83) at long wave-length fluctuations will be the dominant factor in Eq. (82) compared to constant $\kappa_b$. Consequently, the effective bending stiffness at long wave-length fluctuations scales as:

$$\kappa^{\text{eff}}(\mathbf{k}) := \Theta|\mathbf{k}|^{-\zeta} \sim \frac{k_BTE}{\Theta|\mathbf{k}|^{2-\zeta}} \tag{84}$$

from which we obtain the effective bending stiffness as:

$$\kappa^{\text{eff}}(\mathbf{k}) \sim \sqrt{Ek_BT}|\mathbf{k}|^{-1} \tag{85}$$

Using this result we can explore the dependence of the out-of-plane fluctuations on both the characteristic size of the 2D material as well as temperature:

$$\begin{aligned}\langle|w(\mathbf{k})|^2\rangle &\sim \frac{k_BT}{\kappa^{\text{eff}}(\mathbf{k})\mathbf{k}^4}\\ &\sim \frac{1}{L^2|\mathbf{k}|^3}\sqrt{\frac{k_BT}{E}}\end{aligned} \tag{86}$$

The mean-square of the real space out-of-plane fluctuations $\langle w^2\rangle$ is obtained by summing over all possible modes:

$$\begin{aligned}\langle w^2\rangle &\sim \sum_{\mathbf{k}} \frac{1}{L^2|\mathbf{k}|^3}\sqrt{\frac{k_BT}{E}}\\ &\sim \int \frac{2\pi\, kdk}{k^3}\sqrt{\frac{k_BT}{E}}\\ &\sim \frac{1}{k_{\min}}\sqrt{\frac{k_BT}{E}} \sim L\sqrt{\frac{k_BT}{E}}\end{aligned} \tag{87}$$

Here the result from variational perturbation method is different from what is obtained using the naive perturbation expansion.

*6.2.2. Case II: $\varepsilon_0 \neq 0$*

Using similar scaling arguments as before, the effective bending modulus for this case can be expressed as:

$$\kappa^{\text{eff}}(\mathbf{k}) = \kappa_b + \frac{E\varepsilon_0}{(1-\nu^2)|\mathbf{k}|^2} + \frac{\gamma}{|\mathbf{k}|^{2-\zeta}} \tag{88}$$

where $\gamma$—the correction factor—is a constant of no consequence. Given that $\zeta > 0$, the dominant factor in the long wavelength limit is obviously the second term which is proportional to $1/|\mathbf{k}|^2$, $\zeta \approx 2$. Note that this is the same result as what is obtained using regular perturbation method. As intuitive, stretching the sheet results in suppression of out-of-plane fluctuations. Consequently, the nonlinear terms become quite small compared to the quadratic part and hence regular perturbation method is able to yield a reasonable estimate of the out-of-plane fluctuations. This has been also previously explored using the self-consistent screening approximation and Monte Carlo simulations with the conclusion that anharmonic effects are totally suppressed when the in-plane tensile strain is as small as 1% (Roldán et al., 2011).

## 7. Molecular dynamics simulations

To reconcile our analytical calculations with atomistics, we perform MD simulations on monolayer graphene using LAMMPS, an open source code (Plimpton, 1995). The second-generation reactive empirical bond-order (REBO) potential (Brenner et al., 2002) was used for the multibody C–C interactions in graphene.[25] Square-shaped graphene membranes of different linear dimensions were simulated at finite temperatures with periodic boundary conditions. The temperature is controlled by a Nose-Hoover thermostat. Each simulation was run up to 40 ns (time step: 1 fs), with the first 10 ns for the system to equilibrate and the subsequent 30 ns for calculations of the time-averaged quantities. The time integration scheme closely follows the time-reversible measure-preserving Verlet and rRESPA integrators derived by Tuckerman et al. (1992). To simulate monolayer graphene without interlayer interactions, relatively thick simulation boxes were used (thickness $>$ 20 nm). MD simulations with both constant pressure (NPT) and constant volume (NVT) ensembles were performed. In NPT simulations, the dimensions of the simulation box were allowed to change to maintain a constant pressure (or stress). On the other hand, the NVT ensemble was used to simulate graphene subjected to constant area. In both NPT and NVT simulations,

[25] The REBO potential has some limitations even though it was an improvement, in many respects, over the widely used Tersoff force-field and REBO first generation. The second-generation REBO potential takes into account multibody interactions up to third nearest neighbors through the dihedral angles, with which the 4-body interactions are, at least partly, included. As a result, the prediction of the ground-state bending modulus is considerably improved by the second-generation REBO potential as opposed to its first generation counterpart. In the present study, the specific choice of potential (within reason) is not too critical. The focus is on the statistical mechanics analysis of any nonlinear elastic solid membrane. We note that the comparisons with MD simulations are restricted to scaling laws and not actual fluctuations amplitudes. We do not expect scaling laws to be significantly impacted although, certainly, numerical differences in amplitude predictions will depend on the precise potential used. We use the same elastic properties as predicted by the empirical potential at $T = 0$ K in the statistical mechanics analysis. As will be evident from the results in this section, the scaling laws predicted from statistical mechanics theory are in congruence with MD simulations. In summary, although there may exist other potentials that can do even better, the use of the second-generation REBO potential is both convenient (for its availability in LAMMPS) and reasonable for the present study.

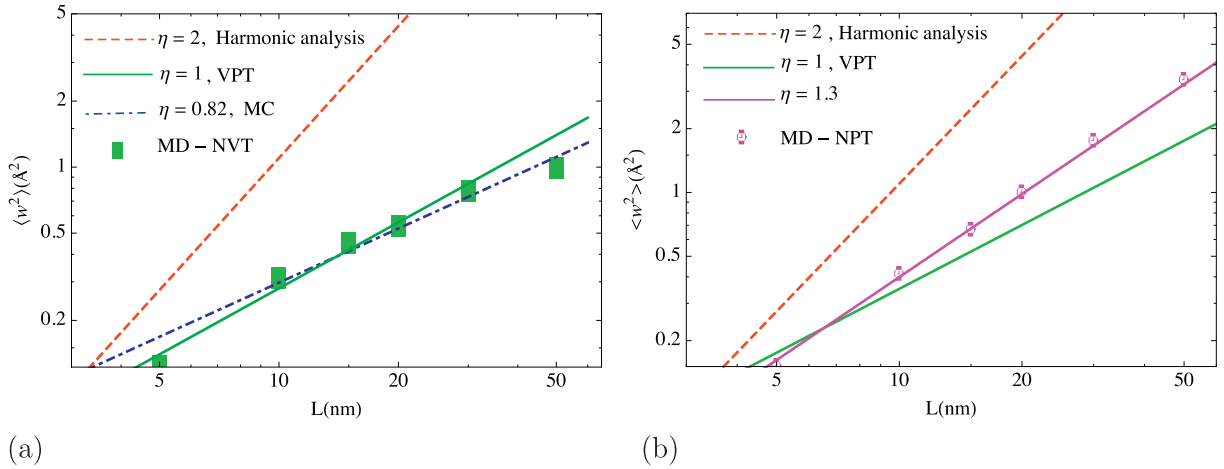


**Fig. 4.** Fluctuation amplitude as a function of a graphene membrane size at $T = 300\,\mathrm{K}$, fitted by the scaling law, $\langle w^2\rangle \propto L_0^{\eta}$, with different exponents obtained from harmonic analysis, variational perturbation approximation (VPT), Monte Carlo (Doussal and Radzihovsky, 1992) and Molecular dynamics simulations under (a) NVT and (b) NPT ensembles.

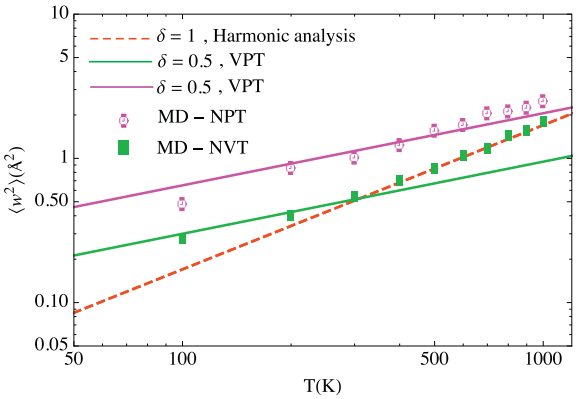


**Fig. 5.** Fluctuations amplitude as a function of temperature, $\langle w^2\rangle \propto T^{\delta}$, with $L_0 = 20\,\mathrm{nm}$.

the mean amplitude of the out-of-plane thermal fluctuation was calculated by a time averaged RMS, namely,

$$\overline{h} = \sqrt{\left\langle \sum_{i=1}^{N} \frac{w_i^2}{N} \right\rangle_t} \tag{89}$$

where $N$ is the total number of atoms and $w_i$ is the out-of-plane displacement of $i$-th atom. Based on the ergodic hypothesis (Weiner, 2012), the time average (over a sufficiently long period) from MD simulation is equivalent to the ensemble average in statistical mechanics. Consequently, the numerical results from MD simulations can be compared directly with the predictions based on statistical mechanics.

Results on the dependency of the out-of-plane displacement field on the temperature and size are shown in Figs. 4 and 5 for both NPT and NVT conditions, where we have compared our results with harmonic approximation as well as the existing models in the literature. In what follows we explain several points regarding our theoretical model in comparison with MD simulations.

## 8. Results and discussion

Unlike in fluid membranes the in-plane and out-of-plane deformations are coupled in solid sheets. As a result of the nonlinear coupling of in- and out-of-plane deformations, the fluctuations in graphene monolayers are found to be suppressed when compared to fluid (biological) membranes (Nelson and Peliti, 1987). Molecular dynamics simulations of graphene monolayers, with periodic boundary conditions in all directions, show that the apparent bending stiffness of graphene at finite temperature is much larger than its bare value at zero kelvin (Doussal and Radzihovsky, 1992; Nelson and Peliti, 1987).

In general, the dependence of the out-of-plane fluctuations can be expressed as:

$$\langle w^2 \rangle \sim L^{\eta} T^{\delta} \tag{90}$$

Comparing Eq. (90) with MD simulations under NPT and NVT ensembles, we highlight the following points here:

- Within the linear framework, as is used for fluid membranes, $\eta = 2$ and $\delta = 1$. Due to nonlinearity, $\eta$ is smaller than 2 for graphene monolayers (Aronovitz and Lubensky, 1988; Doussal and Radzihovsky, 1992; Gao and Huang, 2014; Nelson and Peliti, 1987; Paczuski et al., 1988). Several works have numerically studied this scaling and its entropic consequences (Aronovitz and Lubensky, 1988; Doussal and Radzihovsky, 1992; Gao and Huang, 2014; Nelson and Peliti, 1987; Paczuski et al., 1988). Typical values of $\eta$ for graphene are found to range from 0.7 to 1.2 (Aronovitz and Lubensky, 1988; Doussal and Radzihovsky, 1992; Gao and Huang, 2014; Nelson and Peliti, 1987; Paczuski et al., 1988). In this work, for graphene monolayers, we have obtained $\eta = 1$ and $\delta = 0.5$. These theoretically predicted exponents appear to be in fairly reasonable agreement with our MD simulations. We note that within the NVT ensemble the projected area of the sheet is conserved and hence the kinematics of the deformation is close to that of von-Karman plate theory. The simulations are performed for a limited range of sheet size of graphene (5–50) nm. Within this range, our predictions are consistent with the data from MD simulation results shown in Fig. 4. The results are depicted in log–log scale where the slopes of the straight lines represent the exponent $\eta$. For larger sizes of the graphene sheets (that are not shown in this figure) we speculate that the result corresponding to $\eta = 1$ and obtained from VPT—will diverge from the MD data. In the long-wave length limit, better predictions can be obtained by proceeding to higher order VPT or direct numerical calculations.
- The results for simulations under NPT ensemble are slightly different. This is due to the fact that the NPT simulations are performed such that the in-plane stress field is relaxed. In this manner, the effects of nonlinearities arising from the coupling of in and out-of-plane deformations are softened. Typically, fluctuations under NVT ensemble result in non-zero entropic in-plane stress field (Gao and Huang, 2014). In NPT simulations, the in-plane entropic stresses are relaxed with artificially external compressive forces such that the total stress field becomes zero (Gao and Huang, 2014). As a result of these external compressive forces, the fluctuations are slightly augmented when compared to NVT ensemble.
- The anomalous effects of finite temperature in graphene can be also represented in the so-called *renormalized* or *effective* bending stiffness that depends on the mode of deformation, i.e. $\kappa^{\text{eff}} := \kappa^{\text{eff}}(q)$.[26] The idea is that the bending modulus gets renormalized and diverges at long wave-length fluctuations, stiffening the membrane at large sizes. This was first, studied by Nelson and Peliti (1987) who found that the effective bending stiffness diverges from the bare value of bending modulus $\kappa_b$ for long wave-length fluctuations. Generally, the mode-dependence of $\kappa^{\text{eff}}(q)$ can be expressed as a power law, i.e. $\kappa^{\text{eff}}(q) \sim q^{-\zeta}$. Using a one-loop self-consistent method, Nelson and Peliti (1987) obtained $\zeta = 1$. Later on, several works have revisited this problem using different methods that are well-developed in high-energy physics and statistical field theory literature. Reported values for $\zeta$ in literature range from 0.65 to 1.1 (Aronovitz and Lubensky, 1988; Doussal and Radzihovsky, 1992; Gao and Huang, 2014; Nelson and Peliti, 1987; Paczuski et al., 1988). Using first order regular perturbation *and* a variational based perturbation approach, in this work, we have reexamined this problem. The naive first order perturbation approximation results in a $\zeta = 2$ which is out of the range reported in the literature (Aronovitz and Lubensky, 1988; Doussal and Radzihovsky, 1992; Gao and Huang, 2014; Nelson and Peliti, 1987; Paczuski et al., 1988). We further improve our estimate by employing a variational approach. Up to first order, we have obtained $\zeta = 1$ that is in fairly reasonable agreement with other advanced treatments as well as MD simulations.
  Further, using the fluctuations formulation from VPT and data from MD simulations, we suggest a size-dependent effective bending stiffness that can be cast in the same form as the harmonic approximation:

$$\langle w^2 \rangle = \frac{k_B T L^2}{16\pi^3 \kappa_{\text{eff}}(L)} \tag{91}$$

  where $\kappa_{\text{eff}}$ is assumed to be a function of size of the sheet (L). Based on our prediction from VPT, since the fluctuations vary as $\propto L$, the effective bending stiffness should linearly depend on $L$. A comparison between our estimates and data from MD simulations is made in Fig. 6. As can be observed, the effective bending stiffness obtained for NVT ensemble is larger than for a NPT ensemble. This is again due to the fact that the projected area is fixed within the NVT ensemble which imposes an additional energy cost for out-of-plane deformations. Similar behavior was recently observed in simulations of clamped graphene ribbons (Wan et al., 2017). The clamped boundary conditions tend to fix the projected area of the ribbon. At zero Kelvin, the ribbon is perfectly flat. At finite temperature however, due to out-of-plane deformations the ribbon tends to decrease its projected area. The clamped boundary conditions impose in-plane forces that tend to pull back the area to its initial (zero Kelvin) value. These in-plane entropic forces result in stiffening of the ribbon at finite temperature. As the size of ribbon increases, the out-of-plane fluctuations also increase and hence stronger in-plane forces are required to maintain the fixed projected area. Accordingly, the ribbon is found to be stiffer at larger sizes.
- In Fig. 5, we have also compared our results on the temperature dependency of the fluctuations to MD simulations for a broad range of temperatures (100–1000) K. Our predictions are consistent with data for NVT simulations up to 400 K. However, at higher temperatures the MD results appear to converge to the linear elasticity limit, where $\delta = 1$. This can

[26] Within the harmonic approximation, the effective bending stiffness is simply equivalent to the bare value of the bending modulus and is mode-independent, i.e. $\kappa^{\text{eff}} := \kappa_b$.

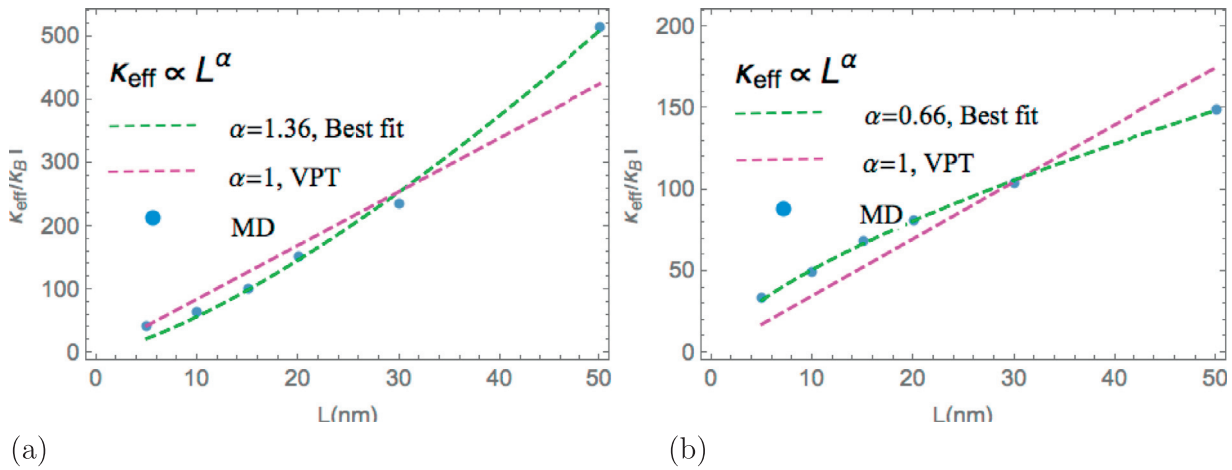


**Fig. 6.** Effective bending stiffness as a function of size is studied for (a) NVT and (b) NPT ensembles at $T = 300$ K. As it is observed the effective bending stiffness increases with the size. The dashed magenta line is our fit using $\alpha = 1$, obtained from VPT. (For interpretation of the references to color in this figure, the reader is referred to the web version of this article.)

be explained by recognizing the fact that at high temperatures, graphene sheet undergoes thermal expansion while the in-plane area is maintained fixed. In this case, the extra area of the graphene sheet resulting from thermal expansion is constrained by compressive forces that attempt to conserve the total in-plane area. Accordingly, the nonlinearities are suppressed.

- The results for NPT ensemble in contrast, are in reasonable agreement with the theoretical predictions even at high temperatures. This is due to the fact that unlike NVT simulations, the area can freely expand at high temperature and hence, the in-plane stress field does not change with the temperature.

We remark that the MD simulations were performed for a limited size range. At larger sizes, not only the fluctuations become far more intense, but also the stiffening effects of nonlinearities are expected to be stronger. For that scenario, the first order approximation of VPT might not yield a reasonable estimate and there may be a need to proceed to higher orders. Using alternative methods it has been shown that the power law of the dependency of the fluctuations on the size of the sheet is different at larger sizes and the exponent $\eta$, converges to the range of 0.8 to 0.85 (Aronovitz and Lubensky, 1988; Doussal and Radzihovsky, 1992; Nelson et al., 2004). On the other hand, the effect of nonlinearity on the temperature dependency of the fluctuations has not been explored theoretically. The first order VPT, however, gives us a reasonable explanation for the temperature dependency of fluctuations as observed in MD simulations. Our estimates in this case, for the reasons described in the preceding paragraphs, are more appropriate for simulations under NPT.

## Acknowledgments

FA gratefully acknowledges discussions with Professor Gemunu Gunaratne. PS and FA acknowledge financial support from the University of Houston M. D. Anderson Professorship and synergistic overlap with work done under NSF CMMI-1463205. PW and RH gratefully acknowledge financial support by the National Science Foundation through Grant no. CMMI-1562820.

## Appendix A. Gaussian integrals

Gaussian integrals are used to calculate the partition functions of harmonic systems. In the following, we briefly summarize the Gaussian integrals for single and multi-variable functions:

- General expression for single variable Gaussian integral:
  This integral is the simplest case, which is used to calculate the partition function for a harmonic oscillator.

$$\int_{-\infty}^{\infty} \mathrm{e}^{-ax^2+bx+c} dx = \sqrt{\frac{\pi}{a}}\ \exp\left(\frac{b^2}{4a} + c\right)$$

- General expression for multi-variable Gaussian integral:
  This integral is used for multiple coupled harmonic oscillators. Consider $n$ different variables, expressed in the function: $f = \frac{1}{2}\sum_{i,j=1}^{n} M_{ij} x_i x_j$, where $M_{ij}$ is coupling coefficient between variable $x_i$ and $x_j$. Now let $M_{ij}$ be the component of the symmetric, positive-definite, $n \times n$ matrix $\mathbf{M}$. Then the corresponding Gaussian integral for the function $f$ is given

as:

$$\int_{-\infty}^{\infty} \exp\left(-\frac{1}{2}\sum_{i,j=1}^{n} M_{ij}x_i x_j\right) d^n x = \sqrt{\frac{(2\pi)^n}{\det \mathbf{M}}} = \sqrt{\det(2\pi \mathbf{M}^{-1})}$$

If a linear term also appears in the function $f$ as: $f = \frac{1}{2}\sum_{i,j=1}^{n} M_{ij}x_i x_j - \sum_{i=1}^{n} B_i x_i$, then the solution to the integration is as follows:

$$\int_{-\infty}^{\infty} \exp\left(-\frac{1}{2}\sum_{i,j=1}^{n} M_{ij}x_i x_j + \sum_{i=1}^{n} B_i x_i\right) d^n x = \sqrt{\frac{(2\pi)^n}{\det \mathbf{M}}} \exp\left(\frac{1}{2}\mathbf{B}^T \mathbf{M}^{-1}\mathbf{B}\right)$$

where $B_i$ are the component of the vector $\mathbf{B}$.

These Gaussian integrals are frequently used in this paper. For example for the case of the one dimensional toy model, the partition function was carried out as follows. Given that $U_b$ is independent of $u_x$, we only need to take into account $U_s$ in the integration over $u_x$. Accordingly, we have:

$$\begin{aligned}
&\prod_{q\in\mathcal{K}_1} \int_{-\infty}^{\infty} \exp\left(-\beta U_s\right) d\overline{u}^{\mathrm{Re}}(q) d\overline{u}^{\mathrm{Im}}(q) \\
&= \exp\left(-\beta \frac{L^2 \overline{E} \varepsilon_0^2}{2}\left(1 + \sum_{q\in\mathcal{K}_1} q^2 |\overline{w}(q)|^2\right)\right) \\
&\quad \times \prod_{q\in\mathcal{K}_1} \int_{-\infty}^{\infty} \exp\left(-\beta \frac{L^2\overline{E}}{2}\left[q\overline{u}^{\mathrm{Re}}(q) + \frac{1}{2}\overline{A}^{\mathrm{Im}}(q)\right]^2\right) d\overline{u}^{\mathrm{Re}}(q) \\
&\quad \times \int_{-\infty}^{\infty} \exp\left(-\beta \frac{L^2\overline{E}}{2}\left[q\overline{u}^{\mathrm{Im}}(q) - \frac{1}{2}\overline{A}^{\mathrm{Re}}(q)\right]^2\right) d\overline{u}^{\mathrm{Im}}(q) \\
&= \exp\left(-\beta \frac{L^2\overline{E}\varepsilon_0^2}{2}\right) \prod_{q\in\mathcal{K}_1} \frac{2\pi}{\beta L^2 \overline{E} q^2} \exp\left(-\frac{\beta L^2 \overline{E}\varepsilon_0}{2} q^2 |\overline{w}(q)|^2\right)
\end{aligned} \tag{92}$$

Given that $\int_{-\infty}^{\infty} \exp(-a(x+b)^2)dx = \sqrt{\pi/a}$, the integration in Eq. (92), becomes independent of $\overline{A}(q)$. Accordingly, $\alpha(q)$ and $U_s^{\mathrm{eff}}$ are given by:

$$\alpha(q) = \frac{2\pi}{\beta L^2 \overline{E} q^2}, \qquad U_s^{\mathrm{eff}} = \frac{L^2 \overline{E}\varepsilon_0}{2}\left(\varepsilon_0 + \sum_{q\in\mathcal{K}_1} q^2 |\overline{w}(q)|^2\right)$$

## Appendix B. Fourier transformation

Fourier transformation can be expressed in terms of sinusoidal functions as:

$$u_x(x) = \sum_{q\in\mathcal{K}_1} a_q \cos(qx) + b_q \sin(qx) \tag{93}$$

On the other hand, given that $\overline{u}^{\mathrm{Re}}(q)$ and $\overline{u}^{\mathrm{Im}}(q)$ are the real and imaginary parts of the $\overline{u}(q)$ we can expand the complex Fourier transform as:

$$\begin{aligned}
u_x(x) &= \sum_{q\in\mathcal{K}_1} \overline{u}(q)\mathbf{e}^{iq\cdot x} \\
&= \sum_{q\in\mathcal{K}_1} (\overline{u}^{\mathrm{Re}}(q) + \mathrm{i}\overline{u}^{\mathrm{Im}}(q))(\cos(qx) + \mathrm{i}\sin(qx)) \\
&= \sum_{q\in\mathcal{K}_1} \overline{u}^{\mathrm{Re}}(q)\cos(qx) - \overline{u}^{\mathrm{Im}}(q)\sin(qx) + \mathrm{i}\sum_{q\in\mathcal{K}_1} (\overline{u}^{\mathrm{Im}}(q)\cos(qx) + \overline{u}^{\mathrm{Re}}(q)\sin(qx))
\end{aligned} \tag{94}$$

We note that for each mode $q$, there is a conjugate mode $-q$, for which we have: $\overline{u}^{\mathrm{Im}}(-q) = -\overline{u}^{\mathrm{Im}}(q)$, $\overline{u}^{\mathrm{Re}}(-q) = \overline{u}^{\mathrm{Re}}(q)$, $\cos(-qx) = \cos(qx)$, and $\sin(-qx) = -\sin(qx)$ which causes the imaginary part of the above summation to vanish. Comparing this summation with the expansion in (93), we can readily relate the coefficients as: $a_q = \overline{u}^{\mathrm{Re}}(q)$ and $b_q = -\overline{u}^{\mathrm{Im}}(q)$.

The derivatives and their corresponding integrations in one dimensional problem can be expressed in Fourier expansion as below:

$$\frac{\partial u_x}{\partial x}=\sum_{q\in\mathcal{K}_1}\mathrm{i}\,q\bar{u}(q)\mathbf{e}^{\mathrm{i}q\cdot x},\qquad \int\left(\frac{\partial u_x}{\partial x}\right)=0,\qquad \int\left(\frac{\partial u_x}{\partial x}\right)^2=L^2\sum_{q\in\mathcal{K}_1}q^2|\bar{u}(q)|^2, \tag{95a}$$

$$\int\left(\frac{\partial^2 w}{\partial x^2}\right)^2=L^2\sum_{q\in\mathcal{K}_1}q^4|\overline{w}(q)|^2,\qquad \int\left(\frac{\partial w}{\partial x}\right)^4=L^2\sum_{q\in\mathcal{K}_1}|\bar{A}(q)|^2 \tag{95b}$$

$$\begin{aligned}\int\frac{\partial u_x}{\partial x}\left(\frac{\partial w}{\partial x}\right)^2&=L^2\sum_{q\in\mathcal{K}_1}\mathrm{i}\,q\bar{u}(q)\bar{A}(-q)=L^2\sum_{q\in\mathcal{K}_1}\mathrm{i}\,q(\bar{u}^{\mathrm{Re}}(q)+\mathrm{i}\,\bar{u}^{\mathrm{Im}}(q))(\bar{A}^{\mathrm{Re}}(-q)+\mathrm{i}\,\bar{A}^{\mathrm{Im}}(-q))\\&=L^2\sum_{q\in\mathcal{K}_1}\mathrm{i}\,q(\bar{u}^{\mathrm{Re}}(q)+\mathrm{i}\,\bar{u}^{\mathrm{Im}}(q))(\bar{A}^{\mathrm{Re}}(q)-\mathrm{i}\,\bar{A}^{\mathrm{Im}}(q))\\&=L^2\sum_{q\in\mathcal{K}_1}q\left(\bar{u}^{\mathrm{Re}}(q)\bar{A}^{\mathrm{Im}}(q)-\bar{u}^{\mathrm{Im}}(q)\bar{A}^{\mathrm{Re}}(q)\right)\end{aligned} \tag{95c}$$

The superscripts "Re" and "Im" denote the decomposition into real and imaginary parts. Also note that we have dropped the imaginary part of the above summation, since it vanishes by summing over the conjugate modes.

For the 2D case also, the corresponding Fourier transformation have real and imaginary parts; i.e. $\bar{\mathbf{u}}(\mathbf{q})=\bar{\mathbf{u}}^{\mathrm{Re}}(\mathbf{q})+\mathbf{i}\,\bar{\mathbf{u}}^{\mathrm{Im}}(\mathbf{q})$, in which the superscripts denote the real and imaginary parts. The corresponding conjugate of each mode is also derived as: $\bar{\mathbf{u}}^*(\mathbf{q})=\bar{\mathbf{u}}(-\mathbf{q})=\bar{\mathbf{u}}^{\mathrm{Re}}(\mathbf{q})-\mathbf{i}\,\bar{\mathbf{u}}^{\mathrm{Im}}(\mathbf{q})$, where $\bar{\mathbf{u}}(\mathbf{q})\bar{\mathbf{u}}^*(\mathbf{q})=|\bar{\mathbf{u}}(\mathbf{q})|^2$. Further, we remark on the orthogonality property of the Fourier modes:

$$\begin{aligned}\int\bar{u}_\gamma(\mathbf{q})\bar{u}_\delta(\mathbf{q}')\mathrm{e}^{i(\mathbf{q}+\mathbf{q}')\cdot\mathbf{x}}d\mathbf{x}&=\delta_{\mathbf{q},-\mathbf{q}'}\bar{u}_\gamma(\mathbf{q})\bar{u}_\delta(\mathbf{q}')L^2\\&=\bar{u}_\gamma(\mathbf{q})\bar{u}_\delta(-\mathbf{q})L^2\end{aligned} \tag{96}$$

Similar arguments can be made for $\bar{A}_{\gamma\delta}(\mathbf{q})$ and $\overline{w}(\mathbf{q})$. Now we can calculate the integration of each terms in $U_{\mathrm{h}}$, $U_{\mathrm{ac}}$ and $U_{\mathrm{anh}}$ in Fourier space. In the following equations, we demonstrate the details of the Fourier transformation of these terms that were not shown in main text of the paper:

$$\int_{\mathbb{S}}\left(\frac{\partial u_\gamma}{\partial x_\delta}\right)^2d\mathbf{x}=L^2\sum_{\mathbf{q}\in\mathcal{K}}q_\delta^2|\bar{u}_\gamma(\mathbf{q})|^2 \tag{97a}$$

$$\int_{\mathbb{S}}\left(\frac{\partial w}{\partial x_\gamma}\frac{\partial w}{\partial x_\delta}\right)^2d\mathbf{x}=L^2\sum_{\mathbf{q}\in\mathcal{K}}|\bar{A}_{\gamma\delta}(\mathbf{q})|^2 \tag{97b}$$

$$\begin{aligned}\int_{\mathbb{S}}\left(\frac{\partial u_\gamma}{\partial x_\delta}\frac{\partial w}{\partial x_k}\frac{\partial w}{\partial x_l}\right)d\mathbf{x}&=L^2\sum_{\mathbf{q}\in\mathcal{K}}\mathbf{i}\,q_\delta\bar{u}_\gamma(\mathbf{q})\bar{A}_{kl}(-\mathbf{q})\\&=L^2\sum_{\mathbf{q}\in\mathcal{K}}q_\delta\left\{\bar{A}_{kl}^{\mathrm{Im}}(\mathbf{q})\bar{u}_\gamma^{\mathrm{Re}}(\mathbf{q})-\bar{u}_\gamma^{\mathrm{Im}}(\mathbf{q})\bar{A}_{kl}^{\mathrm{Re}}(\mathbf{q})+\mathbf{i}\left(\bar{A}_{kl}^{\mathrm{Re}}(\mathbf{q})\bar{u}_\gamma^{\mathrm{Re}}(\mathbf{q})+\bar{u}_\gamma^{\mathrm{Im}}(\mathbf{q})\bar{A}_{kl}^{\mathrm{Im}}(\mathbf{q})\right)\right\}\\&=L^2\sum_{\mathbf{q}\in\mathcal{K}}q_\delta\left\{\bar{A}_{kl}^{\mathrm{Im}}(\mathbf{q})\bar{u}_\gamma^{\mathrm{Re}}(\mathbf{q})-\bar{u}_\gamma^{\mathrm{Im}}(\mathbf{q})\bar{A}_{kl}^{\mathrm{Re}}(\mathbf{q})\right\}\end{aligned} \tag{97c}$$

Note that for each $\mathbf{q}$ mode in the summation, there is a conjugate of $-\mathbf{q}$, that makes the imaginary part of the summation in (97c) vanish:

$$\begin{aligned}&q_\delta\left(\bar{A}_{kl}^{\mathrm{Re}}(\mathbf{q})\bar{u}_\gamma^{\mathrm{Re}}(\mathbf{q})+\bar{u}_\gamma^{\mathrm{Im}}(\mathbf{q})\bar{A}_{kl}^{\mathrm{Im}}(\mathbf{q})\right)+(-q_\delta)\left(\bar{A}_{kl}^{\mathrm{Re}}(-\mathbf{q})\bar{u}_\gamma^{\mathrm{Re}}(-\mathbf{q})+\bar{u}_\gamma^{\mathrm{Im}}(-\mathbf{q})\bar{A}_{kl}^{\mathrm{Im}}(-\mathbf{q})\right)\\&=q_\delta\left(\bar{A}_{kl}^{\mathrm{Re}}(\mathbf{q})\bar{u}_\gamma^{\mathrm{Re}}(\mathbf{q})+\bar{u}_\gamma^{\mathrm{Im}}(\mathbf{q})\bar{A}_{kl}^{\mathrm{Im}}(\mathbf{q})\right)-q_\delta\left(\bar{A}_{kl}^{\mathrm{Re}}(\mathbf{q})\bar{u}_\gamma^{\mathrm{Re}}(\mathbf{q})+(-\bar{u}_\gamma^{\mathrm{Im}}(\mathbf{q}))(-\bar{A}_{kl}^{\mathrm{Im}}(\mathbf{q}))\right)\\&=0\end{aligned} \tag{98}$$

Since, there will not be any contribution from the imaginary parts of the summations, to the free energy, we have taken them out from our calculations.

## Appendix C. Wick's theorem

- Single harmonic oscillator: Consider a single harmonic oscillator of spring stiffness $k$. The potential energy of the spring, when its length is changed by $x$ amount is:

$$U=\frac{1}{2}kx^2$$

Then the higher order correlation function can be calculated as:

$$\langle x^{2n}\rangle = \frac{\int x^{2n} e^{-\beta k x^2/2}}{e^{-\beta k x^2/2}} = (2n-1)\cdot(2n-3)\cdots 5\cdot 3\cdot 1 \frac{1}{(\beta k)^n}$$

Given that $\langle x^2\rangle = 1/\beta k$, the higher order correlation function can be written as:

$$\langle x^{2n}\rangle = (2n-1)!!\langle x^2\rangle^n$$

and this is known as Wick's theorem for a harmonic oscillator. If the potential function is not a quadratic function of $x$, then none of the above expressions are valid. For a set of independent (uncoupled) harmonic oscillators, Wick's theorem can be generalized as following.

- Multi harmonic oscillators: Consider a set of $N$ harmonic oscillators, where $k_i$ is the spring stiffness of the $i$-th oscillator. The total energy is then:

$$U = \sum_{i=1}^{N} \frac{1}{2} k_i x_i^2$$

Note that the oscillators are independent. Each of them behaves like an independent Gaussian integral in the partition function integration:

$$Z = \int e^{-\beta \sum_{i=1}^{N} \frac{1}{2} k_i x_i^2} \prod_{i=1}^{N} dx_i$$

Given that the oscillators are harmonic *and* are not coupled with each other, we have:

$$1) \qquad \langle x_j\rangle = \frac{1}{Z}\int x_j e^{-\beta \sum_{i=1}^{N} \frac{1}{2} k_i x_i^2} \prod_{i=1}^{N} dx_i = \frac{\int x_j e^{-\beta \frac{1}{2} k_j x_j^2} dx_j}{\int e^{-\beta \frac{1}{2} k_j x_j^2} dx_j} = 0$$

$$2) \qquad m \neq n, \quad \langle x_m x_n\rangle = \frac{1}{Z}\int x_m x_n e^{-\beta \sum_{i=1}^{N} \frac{1}{2} k_i x_i^2} \prod_{i=1}^{N} dx_i = \frac{\int x_m e^{-\beta \frac{1}{2} k_m x_m^2} dx_m}{\int e^{-\beta \frac{1}{2} k_m x_m^2} dx_m} \times \frac{\int x_n e^{-\beta \frac{1}{2} k_n x_n^2} dx_n}{\int e^{-\beta \frac{1}{2} k_n x_n^2} dx_n} = 0$$

and in other words, the correlation of two uncoupled harmonic oscillators is always zero. We use this notion to calculate the higher order correlation function:

$$\langle x_{m_1} x_{m_2} x_{m_3} \cdots x_{m_{2n}}\rangle = \frac{1}{Z}\int x_{m_1} x_{m_2} x_{m_3}, \cdots, x_{m_{2n}} e^{-\beta \sum_{i=1}^{N} \frac{1}{2} k_i x_i^2} \prod_{i=1}^{N} dx_i$$

Each of $x_{m_i}$ should be paired with at least one of them to make the above integration nonzero. So we seek all possible pairing options. As example, we start with a set of four oscillators ($x_1$, $x_2$, $x_3$, $x_4$). Then:

$$\begin{aligned} \langle x_1 x_2 x_3 x_4\rangle \neq 0 \quad \text{only if} \quad & x_1 = x_2 \quad \text{and} \quad x_3 = x_4 \\ \text{or} \quad & x_1 = x_3 \quad \text{and} \quad x_2 = x_4 \\ \text{or} \quad & x_1 = x_4 \quad \text{and} \quad x_2 = x_3 \end{aligned}$$

In any other cases, the correlation function $\langle x_1 x_2 x_3 x_4\rangle$ will be zero. Hence, we obtain:

$$\langle x_1 x_2 x_3 x_4\rangle = \langle x_1^2\rangle\langle x_3^2\rangle\delta(x_1,x_2)\delta(x_3,x_4) + \langle x_1^2\rangle\langle x_2^2\rangle\delta(x_1,x_3)\delta(x_2,x_4) + \langle x_1^2\rangle\langle x_2^2\rangle\delta(x_1,x_4)\delta(x_2,x_3)$$

where $\delta$ is the Kronecker delta. Note that a special case of this would be when all the $x_i$ are equal, which reduces to $\langle x^4\rangle = 3\langle x^2\rangle^2$, that has been obtained earlier for the case of single harmonic oscillator.

- Wick's theorem for field theory in Fourier space:

For simplicity, we consider a one dimensional version of the problem in field theory. Consider a beam of size $L$, along the $x$ axis, that can have bending deformation. The elastic bending energy of the beam is assumed to be a quadratic function of the curvature, which, within a linearized approximation can be written in terms of out-of-plane displacement field $h$ as:

$$U = \int \frac{1}{2}\kappa\left(\frac{\partial^2 h}{\partial x^2}\right)^2$$

where $\kappa$ is its bending stiffness. Transforming the displacement field into Fourier space we have:

$$U = L\sum_q \frac{1}{2}\kappa q^4 |\bar{h}_q|^2$$

where, $q$ is the mode number ($2\pi n/L$) and $\bar{h}_q$ is the amplitude of the Fourier transform in mode $q$. In this manner, the total energy looks like the energy of a set of uncoupled harmonic oscillators, with $L\kappa q^4$ being the spring stiffness of the $q$-th oscillator. Accordingly, the correlation functions can be obtained as:

$$1) \quad \langle \bar{h}_q \rangle = 0$$

$$2) \quad \langle \bar{h}_q \bar{h}_{q'} \rangle = \langle |\bar{h}_q|^2 \rangle \delta(q, -q')$$

$$3) \quad \langle \bar{h}_{q_1} \bar{h}_{q_2} \bar{h}_{q_3} \bar{h}_{q_4} \rangle = \langle |\bar{h}_{q_1}|^2 \rangle \langle |\bar{h}_{q_3}|^2 \rangle \delta(q_1, -q_2)\delta(q_3, -q_4) + \langle |\bar{h}_{q_1}|^2 \rangle \langle |\bar{h}_{q_2}|^2 \rangle \delta(q_1, -q_3)\delta(q_2, -q_4) + \langle |\bar{h}_{q_1}|^2 \rangle \langle |\bar{h}_{q_2}|^2 \rangle \delta(q_1, -q_4)\delta(q_2, -q_3)$$

## References


Abbena, E., Salamon, S., Gray, A., 2006. Modern Differential Geometry of Curves and Surfaces with Mathematica. CRC Press.

Ahmadpoor, F., Sharma, P., 2017. A perspective on the statistical mechanics of 2d materials. Extreme Mech. Lett. 14, 38–43.

Ahmadpoor, F., Sharma, P., 2015. Flexoelectricity in two-dimensional crystalline and biological membranes. Nanoscale 7 (40), 16555–16570.

Ahmadpoor, F., Sharma, P., 2016. Thermal fluctuations of vesicles and nonlinear curvature elasticity – implications for size-dependent renormalized bending rigidity and vesicle size distribution. Soft Matter 12 (9), 2523–2536.

Akinwande, D., Brennan, C.J., Bunch, J.S., Egberts, P., Felts, J.R., Gao, H., Huang, R., Kim, J.-S., Li, T., Li, Y., et al., 2017. A review on mechanics and mechanical properties of 2d materials – graphene and beyond. Extreme Mech. Lett.

Aleksandr, I., Khinchin, A., 1949. Mathematical Foundations of Statistical Mechanics. Courier Corporation.

Amit, D.J., Martin-Mayor, V., 2005. Field Theory, the Renormalization Group, and Critical Phenomena: Graphs to Computers. World Scientific Publishing Co. Inc.

Aronovitz, J.A., Lubensky, T.C., 1988. Fluctuations of solid membranes. Phys. Rev. Lett. 60 (25), 2634.

Auth, T., Safran, S., Gov, N.S., 2007. Fluctuations of coupled fluid and solid membranes with application to red blood cells. Phys. Rev. E 76 (5), 051910.

Bhimanapati, G.R., Lin, Z., Meunier, V., Jung, Y., Cha, J., Das, S., Xiao, D., Son, Y., Strano, M.S., Cooper, V.R., et al., 2015. Recent advances in two-dimensional materials beyond graphene. ACS Nano 9 (12), 11509–11539.

Boal, D., Boal, D.H., 2012. Mechanics of the Cell. Cambridge University Press.

Brenner, D.W., Shenderova, O.A., Harrison, J.A., Stuart, S.J., Ni, B., Sinnott, S.B., 2002. A second-generation reactive empirical bond order (rebo) potential energy expression for hydrocarbons. J. Phys. Condens. Matter 14 (4), 783.

Butler, S.Z., Hollen, S.M., Cao, L., Cui, Y., Gupta, J.A., Gutiérrez, H.R., Heinz, T.F., Hong, S.S., Huang, J., Ismach, A.F., et al., 2013. Progress, challenges, and opportunities in two-dimensional materials beyond graphene. ACS Nano 7 (4), 2898–2926.

Canham, P.B., 1970. The minimum energy of bending as a possible explanation of the biconcave shape of the human red blood cell. J. Theor. Biol. 26 (1), 61–81.

Deserno, M., 2007. Fluid Lipid Membranes – A Primer. See http://www.cmu.edu/biolphys/deserno/pdf/membrane_theory.pdf.

Dimova, R., 2014. Recent developments in the field of bending rigidity measurements on membranes. Adv. Colloid Interface Sci. 208, 225–234.

Doussal, P.L., Radzihovsky, L., 1992. Self-consistent theory of polymerized membranes. Phys. Rev. Lett. 69 (8), 1209.

Engelhardt, H., Duwe, H., Sackmann, E., 1985. Bilayer bending elasticity measured by fourier analysis of thermally excited surface undulations of flaccid vesicles. J. Phys. Lett. 46 (8), 395–400.

Farago, O., Santangelo, C.D., 2005. Pore formation in fluctuating membranes. J. Chem. Phys. 122 (4), 044901.

Fasolino, A., Los, J., Katsnelson, M.I., 2007. Intrinsic ripples in graphene. Nat. Mater. 6 (11), 858–861.

Faucon, J., Mitov, M., Méléard, P., Bivas, I., Bothorel, P., 1989. Bending elasticity and thermal fluctuations of lipid membranes. Theoretical and experimental requirements. J. Phys. 50 (17), 2389–2414.

Feng, L., Zhang, S., Liu, Z., 2011. Graphene based gene transfection. Nanoscale 3 (3), 1252–1257.

Fisher, L., 1993. Force between biological surfaces. J. Chem. Soc. Faraday Trans. 89 (15), 2567–2582.

Freund, L., 2013. Entropic pressure between biomembranes in a periodic stack due to thermal fluctuations. Proc. Natl. Acad. Sci. 110 (6), 2047–2051.

Gao, H., 2014. Probing mechanical principles of cell-nanomaterial interactions. J. Mech. Phys. Solids 62, 312–339.

Gao, W., Huang, R., 2014. Thermomechanics of monolayer graphene: rippling, thermal expansion and elasticity. J. Mech. Phys. Solids 66, 42–58.

Goldenfeld, N, 1992. Lectures on Phase Transitions and the Renormalization Group.

Gurtin, M.E., Fried, E., Anand, L., 2010. The Mechanics and Thermodynamics of Continua. Cambridge University Press.

Helfrich, W., 1973. Elastic properties of lipid bilayers: theory and possible experiments. Z. Naturforschung C 28 (11–12), 693–703.

Helfrich, W., 1986. Size distributions of vesicles: the role of the effective rigidity of membranes. J. Phys. 47 (2), 321–329.

Huang, C., Quinn, D., Sadovsky, Y., Suresh, S., Hsia, K.J., 2017. Formation and size distribution of self-assembled vesicles. Proc. Natl. Acad. Sci. 114 (11), 2910–2915.

Kalbacova, M., Broz, A., Kong, J., Kalbac, M., 2010. Graphene substrates promote adherence of human osteoblasts and mesenchymal stromal cells. Carbon 48 (15), 4323–4329.

Kim, K.S., Zhao, Y., Jang, H., Lee, S.Y., Kim, J.M., Kim, K.S., Ahn, J.-H., Kim, P., Choi, J.-Y., Hong, B.H., 2009. Large-scale pattern growth of graphene films for stretchable transparent electrodes. Nature 457 (7230), 706–710.

Kit, O., Tallinen, T., Mahadevan, L., Timonen, J., Koskinen, P., 2012. Twisting graphene nanoribbons into carbon nanotubes. Phys. Rev. B 85 (8), 085428.

Kittel, C., 2004. Elementary Statistical Physics. Courier Corporation.

Kleinert, H., 2009. Path Integrals in Quantum Mechanics, Statistics, Polymer Physics, and Financial Markets. World Scientific.

Koskinen, P., Kit, O.O., 2010. Approximate modeling of spherical membranes. Phys. Rev. B 82 (23), 235420.

Kostarelos, K., Novoselov, K.S., 2014. Exploring the interface of graphene and biology. Science 344 (6181), 261–263.

Kudin, K.N., Scuseria, G.E., Yakobson, B.I., 2001. C 2 f, bn, and c nanoshell elasticity from ab initio computations. Phys. Rev. B 64 (23), 235406.

Kuila, T., Bose, S., Khanra, P., Mishra, A.K., Kim, N.H., Lee, J.H., 2011. Recent advances in graphene-based biosensors. Biosens. Bioelectron. 26 (12), 4637–4648.

Landau, L.D., Lifshitz, E.M., 1959. Course of theoretical physics. Theory and Elasticity, 7. Pergamon Press.

Li, Y., Yuan, H., von dem Bussche, A., Creighton, M., Hurt, R.H., Kane, A.B., Gao, H., 2013. Graphene microsheets enter cells through spontaneous membrane penetration at edge asperities and corner sites. Proc. Natl. Acad. Sci. 110 (30), 12295–12300.

Liang, X., Purohit, P.K., 2016. A fluctuating elastic plate and a cell model for lipid membranes. J. Mech. Phys. Solids 90, 29–44.

Liang, X., Purohit, P.K., 2016. A fluctuating elastic plate model applied to graphene. J. Appl. Mech. 83 (8), 081008.

Lindsay, L., Broido, D., Mingo, N., 2011. Flexural phonons and thermal transport in multilayer graphene and graphite. Phys. Rev. B 83 (23), 235428.

Lipowsky, R., Leibler, S., 1986. Unbinding transitions of interacting membranes. Phys. Rev. Lett. 56 (23), 2541.

Lipowsky, R., Seifert, U., 1991. Adhesion of vesicles and membranes. Mol. Cryst. Liquid Cryst. 202 (1), 17–25.

Lu, Q., Arroyo, M., Huang, R., 2009. Elastic bending modulus of monolayer graphene. J. Phys. D: Appl. Phys. 42 (10), 102002.

Lu, Q., Huang, R., 2009. Nonlinear mechanics of single-atomic-layer graphene sheets. Int. J. Appl. Mech. 1 (03), 443–467.

Mermin, N.D., 1968. Crystalline order in two dimensions. Phys. Rev. 176 (1), 250.

Meyer, J.C., Geim, A.K., Katsnelson, M.I., Novoselov, K.S., Booth, T.J., Roth, S., 2007. The structure of suspended graphene sheets. Nature 446 (7131), 60–63.

Morozov, S., Novoselov, K., Katsnelson, M., Schedin, F., Elias, D., Jaszczak, J.A., Geim, A., 2008. Giant intrinsic carrier mobilities in graphene and its bilayer. Physical Rev. Lett. 100 (1), 016602.
Nayak, T.R., Andersen, H., Makam, V.S., Khaw, C., Bae, S., Xu, X., Ee, P.-L. R., Ahn, J.-H., Hong, B.H., Pastorin, G., 2011. Graphene for controlled and accelerated osteogenic differentiation of human mesenchymal stem cells. ACS Nano 5 (6), 4670–4678.
Nelson, D., Peliti, L., 1987. Fluctuations in membranes with crystalline and hexatic order. J. Phys. 48 (7), 1085–1092.
Nelson, D., Piran, T., Weinberg, S., 2004. Statistical Mechanics of Membranes and Surfaces. World Scientific.
Nelson, P., 2004. Biological Physics. WH Freeman, New York.
Neto, A.C., Guinea, F., Peres, N.M., Novoselov, K.S., Geim, A.K., 2009. The electronic properties of graphene. Rev. Mod. Phys. 81 (1), 109.
Novoselov, K., Jiang, D., Schedin, F., Booth, T., Khotkevich, V., Morozov, S., Geim, A., 2005. Two-dimensional atomic crystals. Proc. Natl. Acad. Sci. USA 102 (30), 10451–10453.
Paczuski, M., Kardar, M., Nelson, D.R., 1988. Landau theory of the crumpling transition. Phys. Rev. Lett. 60 (25), 2638.
Pécréaux, J., Döbereiner, H.-G., Prost, J., Joanny, J.-F., Bassereau, P., 2004. Refined contour analysis of giant unilamellar vesicles. Eur. Phys. J. E 13 (3), 277–290.
Phillips, R., Kondev, J., Theriot, J., Garcia, H., 2012. Physical Biology of the Cell. Garland Science.
Plimpton, S., 1995. Fast parallel algorithms for short-range molecular dynamics. J. Comput. Phys. 117 (1), 1–19.
Roldán, R., Fasolino, A., Zakharchenko, K.V., Katsnelson, M.I., 2011. Suppression of anharmonicities in crystalline membranes by external strain. Phys. Rev. B 83 (17), 174104.
Safran, S.A., 1994. Statistical Thermodynamics of Surfaces, Interfaces, and Membranes, 90. Perseus Books.
Seifert, U., 1997. Configurations of fluid membranes and vesicles. Adv. Phys. 46 (1), 13–137.
Sharma, P., 2013. Entropic force between membranes reexamined. Proc. Natl. Acad. Sci. 110 (6), 1976–1977.
Sun, X., Liu, Z., Welsher, K., Robinson, J.T., Goodwin, A., Zaric, S., Dai, H., 2008. Nano-graphene oxide for cellular imaging and drug delivery. Nano Res. 1 (3), 203–212.
Tuckerman, M., Berne, B.J., Martyna, G.J., 1992. Reversible multiple time scale molecular dynamics. J. Chem. Phys. 97 (3), 1990–2001.
Wan, D., Nelson, D. R., Bowick, M. J., 2017. Thermal Stiffening of Clamped Elastic Ribbons. ArXiv preprint arXiv:1702.01863.
Wang, J., Wei, Y., Shi, X., Gao, H., 2013. Cellular entry of graphene nanosheets: the role of thickness, oxidation and surface adsorption. RSC Adv. 3 (36), 15776–15782.
Wei, Y., Wang, B., Wu, J., Yang, R., Dunn, M.L., 2012. Bending rigidity and gaussian bending stiffness of single-layered graphene. Nano Lett. 13 (1), 26–30.
Weiner, J.H., 2012. Statistical Mechanics of Elasticity. Courier Corporation.
Xu, Z., Buehler, M.J., 2010. Geometry controls conformation of graphene sheets: membranes, ribbons, and scrolls. ACS Nano 4 (7), 3869–3876.
Yang, X., Wang, Y., Huang, X., Ma, Y., Huang, Y., Yang, R., Duan, H., Chen, Y., 2011. Multi-functionalized graphene oxide based anticancer drug-carrier with dual-targeting function and ph-sensitivity. J. Mater. Chem. 21 (10), 3448–3454.
Zakharchenko, K., Roldán, R., Fasolino, A., Katsnelson, M., 2010. Self-consistent screening approximation for flexible membranes: application to graphene. Physical Review B 82 (12), 125435.
Zhong-Can, O.-Y., Helfrich, W., 1989. Bending energy of vesicle membranes: general expressions for the first, second, and third variation of the shape energy and applications to spheres and cylinders. Phys. Rev. A 39 (10), 5280.
Zhu, W., von dem Bussche, A., Yi, X., Qiu, Y., Wang, Z., Weston, P., Hurt, R.H., Kane, A.B., Gao, H., 2016. Nanomechanical mechanism for lipid bilayer damage induced by carbon nanotubes confined in intracellular vesicles. Proc. Natl. Acad. Sci. 113 (44), 12374–12379.